Characteristics of Surface Physical and ~~Biochemical~~Biogeochemical Parameters within Mesoscale Eddies in the Southern Ocean

Qian Liu [1, 2], Yingjie Liu [1, 2], Xiaofeng Li [1, 2]

[1]CAS Key Laboratory of Ocean Circulation and Waves, Institute of Oceanology, Chinese Academy of Sciences, Qingdao 266071, China.
[2]University of Chinese Academy of Sciences, Beijing 100049, China.

Correspondence to: Yingjie Liu (yjliu@qdio.ac.cn)

Abstract. Using satellite sea surface temperature (SST) and chlorophyll-*a* (Chl-*a*) as well as observation-based reconstruction of dissolved inorganic carbon (DIC) and partial pressure of CO_2 (pCO_2) from 1996 to 2015, we investigate the modulation mechanisms of eddies on surface physical and biogeochemical parameters~~analyzed the composite patterns of physical and biochemical variables over eddies~~ in the Southern Ocean (SO). ~~Interestingly, eddy modulation of pCO_2 has marked seasonal and regional variations. The DIC effect dominates the pCO_2 anomalies in winter. In summer, the pCO_2 anomalies within eddies are dominated by DIC (SST) anomalies in regions with larger (smaller) magnitudes of DIC anomalies. In addition, a~~About 1/4 of eddies are observed to be ~~abnormal~~"abnormal" (cold anticyclonic and warm cyclonic eddies) in the SO, which show opposite SST signatures contrary to normal eddies (warm anticyclonic and cold cyclonic eddies). The study finds that t~~T~~he modification of ~~abnormal~~"abnormal" eddies ~~to~~ on physical and ~~biochemical~~biogeochemical parameters is significant~~non-negligible~~ and differs from normal eddies due to the combined~~common~~ effects of eddy pumping and eddy-induced Ekman pumping. ~~For example, DIC anomalies in n~~Normal and ~~abnormal~~"abnormal" eddies have opposite DIC anomalies, contrary to the SST anomalies~~ show dipole patterns with opposite signals~~. ~~Besides~~Moreover, the contributions of ~~abnormal~~"abnormal" eddies to pCO_2 are about 2.7 times higher than normal eddies in regions where ~~abnormal~~"abnormal" eddies dominate. Although Chl-*a* anomalies in normal and "abnormal" eddies show similar patterns and signals, eddy-induced Ekman pumping attenuates the magnitudes of Chl-*a* anomalies within "abnormal" eddies. In addition to the variation of the same parameter within different eddies, the dominant eddy-driven mechanisms for different parameters within the same kind of eddies also vary. The strength of the eddy stirring effect on different parameters is the primary factor causing these differences, attributed to variations in the magnitudes of horizontal parameter gradients~~However, Chl-*a* anomalies in normal and abnormal eddies show similar patterns with the same signals since they are dominated by eddy stirring and pumping~~. Understanding the role of "abnormal" eddies and the complexity of eddy-driven processes is crucial for accurately estimating the influence of mesoscale eddies on physical and biogeochemical processes in the SO, which is essential for simulating and predicting biogeochemical dynamics and carbon cycling in the region.

1 Introduction

Mesoscale eddies are swirling water existingexiting ubiquitously in the global ocean and can influence biochemicalbiogeochemical cycling through horizontal and vertical transport of water masses with physical and biochemicalbiogeochemical parameters (Altabet et al., 2012; Stramma et al., 2013; Dong et al., 2014; Song et al., 2016; Dawson et al., 2018). Eddy activity is particularly high in the Southern Ocean (SO), a critical area fortо global ocean dynamics (Marshall and Speer, 2012). The absorption of anthropogenic CO_2 by the SO accounts for approximately 40 % of the global ocean, and the strength of this carbon sink is variable and sensitive to changes in climate (Le Quéré et al., 2007; Landschützer et al., 2015), highlighting the tremendous importance of SO in the global climate. Therefore, it is significant to comprehensively investigate the role of eddies in regulating physical and biochemicalbiogeochemical parameters in the SO.

Previous literature proposed that eddies influence physical and biochemical parameters through various mechanisms, including eddy stirring, trapping, pumping, and eddy-induced Ekman pumping, and mixing (Chelton et al., 2011; Gaube et al., 2013; Song et al., 2016; Dawson et al., 2018; Frenger et al., 2018). In this study, we revealed how eddies affect sea surface temperature (SST), chlorophyll *a* (Chl *a*), dissolved inorganic carbon (DIC), and partial pressure of CO_2 (pCO_2) through these mechanisms.

Eddy stirring and trapping are two mechanisms that redistribute physical and biochemical parameters spatially through horizontal advection. Eddy stirring refers to the local deformation of a large-scale horizontal parameter gradient via eddy rotation, resulting in dipole patterns of eddy-induced physical and biochemical parameters (Chelton et al., 2011; Frenger et al., 2015; Dawson et al., 2018; Frenger et al., 2018). For instance, under the northward increasing chlorophyll *a* (Chl *a*) gradient, anticyclonic eddies (AEs), which rotate counterclockwise in the Southern Hemisphere, would advect high Chl *a* from the north to the southwest and low Chl *a* from the south to the northeast. The reverse is true for cyclonic eddies (CEs) in the Southern Hemisphere. Besides, eddy trapping refers to the advective transport water masses with physical and biochemical parameters and tends to cause monopole patterns, which are determined by the directions of horizontal parameter gradient and eddy propagation (Chelton et al., 2011; Gaube et al., 2014; Mcgillicuddy, 2016). For example, under the southward increasing Chl *a* gradient, northward/southward propagating AEs/CEs trap high/low Chl *a*, inducing monopole positive/negative Chl *a* anomalies.

Eddy pumping and, eddy-induce Ekman pumping, and mixing are the other two mechanisms that modulate and redistribute physical and biochemical parameters through vertical transports in eddy cores. Eddy pumping refers to the vertical displacement of isopycnals during the formation, growth, and destruction of mesoscale eddies (Huang et al., 2017; Dawson et al., 2018; Xu et al., 2019). Typically, AEs cause a deepening of isopycnals and downwelling with unproductive water. On the contrary, CEs lead to a doming of isopycnals and upwelling with cold, nutrient-rich deep water into the euphotic zone (Mcgillicuddy and Robinson, 1997; Mcgillicuddy et al., 1998; Nencioli et al., 2010; Lasternas et al., 2013). Therefore, eddy pumping causes negative Chl *a* anomalies within AEs and positive Chl *a* anomalies within CEs. However, recent studies have reported that eddy induce Ekman pumping leads to the opposite effect with positive (negative) Chl *a*

~~anomalies in AEs (CEs) (Gaube et al., 2013; Gille et al., 2014; Dawson et al., 2018). Eddy-induced Ekman pumping is generated by sea surface stress curl caused by surface differential currents associated with mesoscale eddies and surface wind fields (Gaube et al., 2015). This surface stress curl has an opposite polarity to the vorticity of the eddy and thus generating Ekman upwelling (downwelling) in the cores of AEs (CEs).~~

~~Mesoscale eddies regulate SST, Chl-*a*, and DIC through these four mechanisms, affecting pCO_2 (Frenger et al., 2013; Song et al., 2016). Previous findings indicated that the pCO_2 is positively correlated with SST and DIC but negatively correlated with Chl-*a* (Chen et al., 2007; Landschützer et al., 2015; Song et al., 2016; Jersild and Ito, 2020; Iida et al., 2021). Besides, the competing seasonal cycles of SST, Chl-*a*, and DIC affect the seasonal variability of pCO_2 (Jiang et al., 2014; Munro et al., 2015; Jersild and Ito, 2020). For example, in summer, strong biological utilization of carbon causes the minimum surface DIC and pCO_2 (Takahashi et al., 2009; Munro et al., 2015; Fay et al., 2018; Jersild and Ito, 2020). On the contrary, the warm SST lowers the solubility and thus elevates pCO_2. In winter, pCO_2 increases due to the suppression of biological productivity and upwelling deep waters with high concentrations of DIC (Landschützer et al., 2015; Fay et al., 2018; Jersild and Ito, 2020). However, cold SST leads to higher solubility and thus decreases pCO_2.~~

~~Moreover, previous studies found that the seasonal variation of pCO_2 within the eddies varies in different regions. For example, in the Drake Passage between the Atlantic and Pacific sectors of the SO, Song et al. (2016) found that AEs/CEs have negative/positive pCO_2 anomalies in summer, contrary to winter. They suggested that pCO_2 within eddies is dominated by DIC (SST) in summer (winter). However, in the Georgia Basin, the Atlantic sector of the SO, Jones et al. (2017) found that both AEs and CEs have negative pCO_2 anomalies dominated by DIC in summer. Within CEs, upwelled nutrient supply increased biological productivity, which counteracted DIC inputs from deep waters. This result is contrary to that reported by Song et al. (2016). In other regions, researchers also found different effects of eddies on pCO_2 (Chen et al., 2007; Frenger et al., 2013). For instance, the pCO_2 in CEs increases in the subtropical North Pacific Gyre and decreases in the SO. These findings illustrate that the mechanisms of eddy-induced modifications to pCO_2 vary by season and region.~~ Sea surface temperature (SST), chlorophyll-*a* (Chl-*a*), dissolved inorganic carbon (DIC), and partial pressure of CO_2 (pCO_2) are crucial physical and biochemical parameters that are extensively utilized to investigate the impact of mesoscale eddies on the marine environment and carbon cycle (Mcgillicuddy and Robinson, 1997; Gaube et al., 2013; Frenger et al., 2015; Jones et al., 2017). Previous literature found eddies can deform the horizontal parameter gradient via eddy rotation (eddy stirring), trap and transport water masses (eddy trapping), and enhance or suppress local surface SST, Chl-*a*, DIC, and pCO_2 through the vertical velocity in eddy cores, such as eddy pumping, seasonal modulation of the mixed layer, and eddy-induced Ekman pumping (Mcgillicuddy et al., 2007; Dufois et al., 2014; Gaube et al., 2014; Song et al., 2016; Dawson et al., 2018; Frenger et al., 2018). Eddy pumping refers to the vertical displacement of isopycnals during the formation, growth, and destruction of mesoscale eddies (Nencioli et al., 2010; Lasternas et al., 2013; Huang et al., 2017; Dawson et al., 2018; Xu et al., 2019). Typically, anticyclonic eddies (AEs) cause a deepening of isopycnals and downwelling with warm, unproductive, and low-DIC surface water. On the contrary, cyclonic eddies (CEs) lead to a doming of isopycnals and upwelling with cold, productive, and DIC-rich deep water into the euphotic zone. The variation of pCO_2 was found to be positively correlated

with SST and DIC but negatively correlated with Chl-*a* (Chen et al., 2007; Frenger et al., 2013; Landschützer et al., 2015; Song et al., 2016; Jones et al., 2017; Fay et al., 2018; Jersild and Ito, 2020; Iida et al., 2021). Therefore, the variation of pCO_2 within the eddies will be complex and necessitates discussion based on seasons and regions.

However, recent studies have reported that seasonal modulation of the mixed layer and eddy-induced Ekman pumping can cause eddy-induced anomalies contrary to those predicted due to unusual vertical transports in eddy cores (Mcgillicuddy et al., 2007; Gaube et al., 2013; Dufois et al., 2014; Gaube et al., 2014; Gille et al., 2014; Dawson et al., 2018). For example, Dufois et al. (2014) suggested that in the South Indian Ocean between 20°S and 30°S, deeper mixing in winter AEs can elevate nutrient supply, while shallower mixing in CEs can reduce it, which could explain stronger positive Chl-*a* anomalies in AEs than in CEs. The influence of mixing on Chl-*a* anomalies within eddies is similar to the eddy-induced Ekman pumping, which is generated by the sea surface stress curl caused by surface differential currents associated with mesoscale eddies and surface wind fields (Mcgillicuddy et al., 2007; Gaube et al., 2015). This surface stress curl has an opposite polarity to the vorticity of the eddy, causing Ekman upwelling in the cores of AEs and Ekman downwelling in the cores of CEs. Unlike the seasonal modulation of the mixed layer, eddy-induced Ekman pumping persists throughout the lifetime of the eddy, and its magnitude depends on eddy amplitude and ambient wind speed (Gaube et al., 2014).

~~In addition~~Previous research has primarily utilized rotation direction and sea surface height anomaly (SSHA) to distinguish AEs and CEs and analyze their impacts on physical and biochemical parameters (Frenger et al., 2015; Song et al., 2016; Dawson et al., 2018). However, recent studies found that AEs can be further divided into warm and cold anticyclonic eddies (WAEs and CAEs). Similarly, CEs can be divided into cold and warm cyclonic eddies (CCEs and WCEs) depending on SST (Leyba et al., 2017; Liu et al., 2020; Liu et al., 2021; Ni et al., 2021). ~~Consequently,~~ WAEs and CCEs are considered normal eddies that align with~~obey~~ conventional knowledge, and CAEs and WCEs are considered ~~abnormal~~"abnormal" eddies. ~~Abnormal~~"Abnormal" eddies are ubiquitous in the ocean, constituting approximately ~~accounting for about~~ 32 % of the total eddies in the global ocean, and ~~abnormal~~"abnormal" eddies in the Antarctic Circumpolar Current (ACC) account for 19.9 % of ~~the~~ global ~~total abnormal~~"abnormal" eddies (Liu et al., 2021). Previous literature proposed that "abnormal" eddies may be induced by eddy-induced Ekman pumping (Gaube et al., 2013; Mcgillicuddy, 2015), instability during the eddy decay stage, eddy horizontal entrainment (Sun et al., 2019), and warm/cold background water (Leyba et al., 2017). ~~Moreover, t~~The roles of ~~abnormal~~"abnormal" eddies in ocean circulation (Shimizu et al., 2001), mass transportation (Pickart et al., 2005; Mathis et al., 2007; Everett et al., 2012), and air-sea interaction (Leyba et al., 2017; Liu et al., 2020) ~~are~~ differ~~ent~~ from those of normal ones (Assassi et al., 2016; Dilmahamod et al., 2018). ~~For example, Pezzi et al. (2021) found a WCE causing the ocean to act locally as a CO_2 source, contrary to the previous result that CCEs act locally as CO_2 sinks (Chen et al., 2007; Frenger et al., 2013; Jones et al., 2017). The case study preliminarily shows the difference between normal and abnormal eddies on pCO_2.~~ However, the specific impact of "abnormal" eddies on physical and biogeochemical parameters in the SO remains unclear~~how abnormal eddies in the SO affect physical and biochemical parameters remains unclear~~. Moreover, previous studies have primarily focused on the basin-wide effects of eddies on Chl-*a*, while investigations into the basin-scale effects of SO eddies on DIC and pCO_2 are lacking. Given the potential interactions between different physical and

biogeochemical parameters and the importance of the SO in global climate change, biological productivity, and carbon cycling, it is necessary to systematically study the influence of eddies on SST, Chl-*a*, DIC, and pCO_2 in the SO.

~~Previous studies of eddy-induced anomalies in the SO focused on the advective effects of eddies on Chl-*a* and did not distinguish between normal and abnormal eddies (Frenger et al., 2015; Frenger et al., 2018). However, abnormal eddies have SST anomalies opposite to normal eddies, which can potentially affect the biochemical parameters within eddies. Therefore,~~ ~~w~~We aim to extend SO eddy-induced anomalies studies and examine the influence of ~~abnormal~~"abnormal" eddies on surface physical and ~~biochemical~~biogeochemical parameters. Unlike traditional eddy detection methods based on satellite sea surface height (SSH) data (Chelton et al., 2011a; Faghmous et al., 2015), the eddy dataset we used is developed by a deep learning (DL) model based on the fusion of SSH and SST data (Liu et al., 2021), which can simultaneously detect eddy locations and distinguish between normal and "abnormal" eddies with great accuracy and efficiency. Instead of using potential density and geostrophic current direction to identify "abnormal" eddies (Mcgillicuddy, 2015), we choose to use the SST signature for distinguishing between normal and "abnormal" eddies. Because compared to potential density, SST data can be obtained from satellite remote sensing with higher spatial and temporal resolutions, making it a convenient and reliable data source for identifying eddies (Castellani, 2006; Liu et al., 2021). Using satellite SST and Chl-*a*, observation-based reconstruction of DIC and pCO_2, and eddy datasets from 1996 to 2015, we systematically analyze their seasonal and regional variations induced by normal and ~~abnormal~~"abnormal" eddies and investigate~~examine~~ the mechanisms driving these responses. The study is organized as follows (Fig. S1). First, Sects. 2 and 3 provide details about~~present~~ data and methods. Then, in Sect. 4, we present the spatial distributions of eddy parameters, as well as spatial distributions and composite maps of eddy-induced SST, Chl-*a*, DIC, and pCO_2 anomalies. Section 5 investigat~~discuss~~es the mechanisms driving the surface parameter~~s~~'s responses to eddies. Section 6 discusses the cause of distinct dominant eddy-driven mechanisms for different parameters within the same kind of eddies and provides conclusions~~Finally, we conclude in Sect. 6~~.

2 Data

2.1 Study region

The SO is the region between 30°S and 65°S (Fig. 1~~2~~). The ACC in the SO is a global circulation that links the Pacific, Atlantic, and Indian Oceans from west to east (Marshall and Speer, 2012). We use~~d~~ the positions of the northern Subantarctic Front (SAF) and the Polar Front (PF) (Sallée et al., 2008) available from the Center for Topographic Studies of the Ocean and Hydrosphere (CTOH; http://ctoh.legos.obs-mip.fr/applications/mesoscale/southern-ocean-fronts). We average~~d~~ the data of the fronts over the eddy period (1996 to 2015) as boundaries for ACC major Fronts (black lines in Fig. 1~~2~~).

2.2 SST, Chl-*a*, DIC, and pCO_2 datasets

Four datasets of sea surface parameters are used in the study, including SST, Chl-*a*, DIC, and pCO_2 from 1996 to 2015, between 30°S and 65°S. A brief description of each data is given below.

The daily SST dataset is the NOAA Optimum Interpolation (OI) SST product with 0.25° resolution, spanning from 1981 to the present (Reynolds et al., 2007). The ~~OI~~SST dataset combines observations from different platforms on a regular global grid, including Advanced Very High-Resolution Radiometer (AVHRR) satellite data, ships, buoys, and Argo floats with an accuracy of about 0.1 °C daily.

The Chl-*a* dataset is provided by Copernicus Marine Environmental Monitoring Service (CMEMS), based on the Copernicus-GlobColour processor that merges three algorithms (Gohin et al., 2002; Hu et al., 2012; Garnesson et al., 2019). The Chl-*a* dataset combines observations from different sensors (SeaWiFS, MODIS Aqua, MODIS Terra, MERIS, VIIRS NPP, VIIRS-JPSS1 OLCI-S3A, and S3B). The original 4 km resolution data was re-gridded to 0.25° with daily temporal resolution. We log-transform Chl-*a* using the base 10 logarithm because Chl-*a* is lognormally distributed (Campbell, 1995).

The pCO_2 and DIC datasets are from the Japan Meteorological Agency (JMA) Ocean CO_2 Map dataset with monthly 1° × 1° gridded values on the global ocean from 1990 to 2020 (Iida et al., 2021). The DIC concentration is calculated from total alkalinity (TA) values and CO_2 fugacity (fCO_2) data provided by the Surface Ocean CO_2 Atlas (SOCAT), containing data from the 1950s to the present (Bakker et al., 2016). The DIC field is gap-filled~~estimated~~ by using a multi-linear regression (MLR) method based on the DIC and satellite observation data, including SST, sea surface salinity (SSS), sea surface dynamic height (SSDH), Chl-*a*, and surface mixed layer depth (MLD) (Iida et al., 2021).

$$nDIC = f(\text{time, SST, SSS, SSDH, Chl-}a\text{, MLD}), \quad (1)$$

The globally averaged error in DIC ~~was~~is 6.1 μmol kg^{-1}, which is 5.4 μmol kg^{-1} smaller than the error of Global Ocean Data Analysis Project version 2 update 2019 (GLODAPv2.2019), a uniformly calibrated open ocean data product on inorganic carbon and carbon-relevant variables (Olsen et al., 2019).

The pCO_2 field is ~~then~~ calculated from TA, DIC, SST, and SSS based on seawater CO_2 chemistry (Iida et al., 2021). Firstly, the mean rates of regional pCO_2 and multiple regressions are used to derive the algorithms of pCO_2 expressed empirically as a function of in situ TA, DIC, SST, SSS, and the year. Then, the pCO_2 fields that filled both in space (1° × 1°) and time (monthly) are drawn by applying global data sets of TA, DIC, SST, and SSS to the variables in these empirical equations. ~~The globally averaged error in DIC was 6.1 μmol kg^{-1}, which is 5.4 μmol kg^{-1} smaller than the error of Global Ocean Data Analysis Project version 2 update 2019 (GLODAPv2.2019), a uniformly calibrated open ocean data product on inorganic carbon and carbon-relevant variables (Olsen et al., 2019). Moreover, t~~The error in pCO_2 was 10.9 μatm, comparable with those estimated with other empirical methods, e.g., 14.4 μatm (Landschützer et al., 2014) and 15.73 μatm (Denvil-Sommer et al., 2019). This dataset developed by Iida et al. (2021) is widely used to study the relationship between the pCO_2 low-frequency variability and the recent global warming hiatus and the Interdecadal Pacific Oscillation, the net

带格式的: 缩进:首行缩进: 1 字符

community production and ocean acidification ~~the relationship between pCO_2 and physical and biochemical parameters such as biological productivity, heat, and typhoons~~ (Hashihama et al., 2021; Qiu et al., 2021; Ono et al., 2023).

2.3 Eddy Database

Normal and ~~abnormal~~"abnormal" eddies are from the eddy dataset developed by Liu et al. (2021)~~were identified by~~, using a deep learning (DL) model based on the fusion of satellite sea surface height (SSH) and SST data ~~(Liu et al., 2021)~~. Based on the U-Net framework (Ronneberger et al., 2015; Falk et al., 2019), the model combines HyperDense-Net (Dolz et al., 2019) to fuse SSH and SST data. The SSH data used in the model is obtained from the Archiving, Validation, and Interpretation of Satellite Oceanographic (AVISO) dataset. The SST data refers to the NOAA ~~OI~~SST product (Reynolds et al., 2007). ~~The eddy data set is a daily and 0.25° resolution, including the number, radius, amplitude, rotational speed, and eddy kinetic energy (EKE) in the global ocean from 1996 to 2015. Besides, t~~The model simultaneously extracts SSH anomaly (SSHA) features ~~for~~ to ~~determining~~ determine eddy locations and distinguish between AEs and CEs and extracts the mean SST anomaly (SSTA) within eddy boundaries~~information~~ to distinguish between normal and ~~abnormal~~"abnormal" eddies. Specifically, WAEs are identified according to SSHA >0 and SSTA >0, CAEs are identified according to SSHA >0 and SSTA <0, CCEs are identified according to SSHA <0 and SSTA <0, and WCEs are identified according to SSHA <0 and SSTA >0. The dice loss (a cost function to calculate the difference between the predicted and true values) and accuracy of the model was about 14 % and 94 % when training with the ground truth data set, generated automatically using the SSH-based method (Liu et al., 2016). The eddy data set has a daily and 0.25° resolution, including the number, radius, amplitude, rotational speed, and eddy kinetic energy (EKE) in the global ocean from 1996 to 2015. ~~However, d~~Due to the limitations of the resolution capability of the SSHA data (Ducet et al., 2000), eddies with amplitudes < 2 cm and radii < 35 km were discarded in this work.

Compared to the AVISO eddy database (Pegliasco et al., 2022), our study utilizes a different eddy detection method (Liu et al., 2021). The reason why we use this method is that DL technology has unparalleled learning ability and the capability to model complex nonlinear relationships compared to traditional statistics and machine learning methods (Reichstein et al., 2019). Besides, our method achieves great accuracy and much higher efficiency than the traditional method that first detects the eddies and then uses the SST signature to classify them into normal and "abnormal" eddies. In addition, the method is able to detect eddies in regions where traditional methods may not be effective, such as in regions with weak eddies or regions with complex oceanic dynamics (Liu et al., 2021). Given its high accuracy and comprehensive information on eddy characteristics, we find this dataset particularly useful for our study. Considering that the changes in SSH, SST, Chl-*a*, and roughness caused by eddies can be recorded by altimeter, infrared, ocean color, and synthetic aperture radar (SAR) remote sensing, respectively, and potential density and temperature recorded by Argo floats can also identify "abnormal" eddies, in future work, we will combine multiple remote sensing data with Argo profiles to evaluate the accuracies of "abnormal" eddy identification method.

带格式的: 缩进:首行缩进: 1 字符

3 Eddy Analysis Methodology

3.1 ~~Eddy-centric Composite Method~~Composite Eddy-induced Anomalies

To extract the eddy-induced mesoscale features in sea surface variables, including SST, Chl-*a*, DIC, and pCO_2, we use~~d~~ temporal and spatial filters similar to those used in Villas Bôas et al. (2015) (Fig. S2~~3~~). The temporal filter is a band-pass Butterworth window (Butterworth, 1930) applied to preserve the temporal signal between 7 and 90 days corresponding to the typical time scales of the eddies. The SST and Chl-*a* anomalies are computed using the 7-90 days band-pass filter to remove the seasonal signal. However, for DIC and pCO_2 datasets with the monthly temporal resolution, we subtract their climatological averages. The spatial filter is a moving average Hann window (Stearns and Ahmed, 1976) designed to contain spatial signals smaller than 600 km. This filter removes ~~the~~ large-scale variability unrelated to the mesoscale eddy influence.

Finally, we use the eddy-centric composite method to estimate the spatial pattern of the eddy-induced anomalies in sea surface variables. The positions of co-located SST, Chl-*a*, DIC, and pCO_2 observations are normalized by R, which defines the edge of an eddy as ±1 and the eddy core as 0. This allows us to construct composite averages from eddies of various sizes. We then extract data from −2R to 2R to include the interactions between eddies and the surrounding waters and interpolate them onto an evenly spaced 17 by 17 grid to create the surface composite patterns. For daily SST and Chl-*a*, we perform the eddy-centric composite method matching eddies and variables on the same day and calculate the mean value. In contrast, for monthly DIC and pCO_2, we calculate the eddy-centric composite maps using all eddies of the same month, along with DIC and pCO_2 data from that month, and obtain the mean value. The composite maps are not rotated with the background variables gradient, as the large-scale background variables gradients in the SO are predominantly oriented north-south. Previous studies have indicated that rotating eddies to the large-scale variables gradient in the SO has a negligible impact on the results (Frenger et al., 2015). Therefore, the axes in each figure point north and east. This eddy-centric composite method is frequently used in studies of eddy tracer anomalies (Hausmann and Czaja, 2012; Gaube et al., 2013; Gaube et al., 2014; Frenger et al., 2015; Gaube et al., 2015; Dawson et al., 2018). Its advantage lies in the ability to average over multiple eddies, which helps reduce noise and reveal persistent eddy structures (Melnichenko et al., 2017). This method is particularly useful when studying eddies in regions where eddy activity is highly variable, as it allows us to identify common patterns and trends in eddy-induced anomalies.~~Finally, the spatial pattern of the eddy-induced anomalies in sea surface variables was estimated using composite maps. For each identified eddy with a radius of R, the eddy-induced anomalies were mapped onto the eddy-centric coordinate spanning 2R. The advantage of the eddy-centric composite method is that averaging over many eddies helps suppress noise and reveal persistent eddy structures (Melnichenko et al., 2017).~~

3.2 Eddy-induced Ekman pumping

At present, there are no explicit formulas to quantify eddy stirring, trapping, and pumping, but with the Ekman transport modified by the surface geostrophic vorticity ζ following Stern (1965), the total eddy-induced Ekman pumping W_{tot} is

$$W_{tot} = \frac{1}{\rho_o}\nabla \times \left[\frac{\boldsymbol{\tau}}{(f+\zeta)}\right] \approx \frac{\nabla \times \boldsymbol{\tau}}{\rho_o (f+\zeta)} + \frac{1}{\rho_o (f+\zeta)^2}\left(\tau^x \frac{\partial \zeta}{\partial y} - \tau^y \frac{\partial \zeta}{\partial x}\right), \quad (2)$$

where ρ_o = 1020 kg m^{-3} is the (assumed constant) density of sea surface water, f is the Coriolis parameter, and the surface stress $\boldsymbol{\tau}$ has zonal and meridional components τ^x and τ^y, respectively. The surface stress curl $\nabla \times \boldsymbol{\tau}$ was computed by using finite centered differences of τ^x and τ^y. The surface geostrophic vorticity ζ is calculated as

$$\zeta = \frac{\partial v}{\partial x} - \frac{\partial u}{\partial y}, \quad (3)$$

where u and v are the zonal and meridional components of geostrophic current velocity. The surface wind stress $\boldsymbol{\tau}$ is calculated as

$$\boldsymbol{\tau} = \rho_a C_D (U_a - U_o)|U_a - U_o|, \quad (4)$$

where ρ_a = 1.2 kg m^{-3} is the air density (assumed constant), C_D is the drag coefficient, U_a and U_o are the wind and ocean current vectors, respectively. The above formulas to calculate the W_{tot} are similar to those used in Gaube et al. (2015).

U_a is a gridded Level 4 (L4) product with 0.25° resolution available every six hours from the Cross-Calibrated Multi-Platform (CCMP) ocean surface wind data set, produced by Remote Sensing Systems. The data set combines ocean surface (10m) wind retrievals from a reanalysis background field from the ERA-Interim reanalysis, multiple types of satellite microwave sensors, and observations from ships and buoys. The U_o is a daily sea surface geostrophic current product with a spatial 0.25° resolution obtained from AVISO.

To extract the mesoscale features of W_{tot}, we used temporal and spatial filters similar to those used in Gaube et al. (2015). In addition, tThe W_{tot} was is temporally low-pass filtered with a half-power filter cutoff of 30 days and spatially high-pass filtered to contain spatial signals smaller than 600 km. Finally, we use the eddy-centric composite method to obtain the spatial pattern of eddy-induced Ekman pumping.

4 Results

4.1 Spatial Distributions of Normal and Abnormal"Abnormal" Eddies

From 1996 to 2015, an average of 1991 eddies were identified daily in the SO (65°S–30°S), with abnormal"abnormal" eddies accounting for 26.3 % of the total. Figures 24a, b, d, and e show the spatial distribution of eddy number, defined as the frequency of eddies eddy occurrence in each 1° × 1° latitude-longitude bin over the analyzed period 1996–2015. The eddy frequency represents the ratio of the number of days eddies appeared to the total number of observation days. Eddies disappear in the regions shallower than 2000m and the area near Antarctica (shown in gray in Fig. 24) because the bottom topography constrains the generation of eddies, and satellite altimetric cannot measure sea level beneath sea ice (Frenger et

al., 2015). Normal and ~~abnormal~~"abnormal" eddies are concentrated in ~~the~~ strong currents regions, such as the ACC, Western Boundary Current (WBC), and Eastern Boundary Current (EBC) regions, as shown in Fig. 1~~2~~. These finding~~Such~~ ~~result~~s are consistent with those findings reported by Frenger et al. (2015), which did not distinguish between normal and ~~abnormal~~"abnormal" eddies. The differences between AEs and CEs, i.e., the eddy polarity, are critical for understanding the~~eddy-induced~~ physical and ~~biochemical~~biogeochemical anomalies induced by eddie (Mcgillicuddy et al., 1998; Siegel et al., 2011). ~~Abnormal~~"Abnormal" eddies have the opposite polarity distribution to normal eddies in the continental boundary currents where more CCEs and CAEs occur. The most significant difference ~~between~~ in ~~the~~ polarity distributions ~~of~~ between normal and ~~abnormal~~"abnormal" eddies is the dominance of WAEs and WCEs in the southwestern Australia (SWA) (Figs. 2~~4~~c, f).

Despite the great differences in ~~the~~ occurrence distributions ~~of four kinds of eddies~~, the~~ir~~ amplitude distributions of the four types of eddies are similar. The eddy amplitude is greater in the Brazil Malvinas Confluence (BMC), Agulhas Return Current (ARC), ACC, SWA, and Tasman S~~s~~ea (Figs. 2~~4~~g, h, j, and k). One should note that the amplitudes of ~~abnormal~~"abnormal" eddies are smaller than ~~their~~ those of normal ones (Table S1), which is consistent with previous studies (Liu et al., 2020; Liu et al., 2021). In addition, the spatial distributions of rotational speed and EKE correlate well with the patterns of eddy amplitude ~~patterns~~ (Fig. S3~~5~~).

4.2 Spatial Distributions of Eddy-induced SST, Chl-*a*, DIC, and pCO_2 Anomalies

Using the eddy-centric composite method (Fig. S2~~3~~), we average~~d~~ the eddy-induced SST, Chl-*a*, DIC, and pCO_2 anomalies into 1° × 1° longitude-latitude grid boxes. The maps of the climatological imprint of eddies on SST show that the distributions of SST anomalies over normal eddies ~~are well~~ correlate well~~d~~ with the amplitude distributions, with stronger positive/negative SST anomalies (in WAEs/CCEs) concentrated in the BMC, ARC, ACC, SWA, and Tasman S~~s~~ea (Figs. 3~~6~~a, c). In contrast, in ~~the~~ regions with larger amplitudes, CAEs/WCEs have weaker negative/positive SST anomalies (Figs. 3~~6~~b, d).

Also, the distributions of Chl-*a* anomalies over both normal and ~~abnormal~~"abnormal" eddies are similar to the amplitude distributions, with stronger negative/positive anomalies within AEs/CEs in regions ~~of~~ with higher amplitudes (Figs. 3~~6~~c–h). However, in the south of the ACC, including the ACC, we ~~found~~ find the patterns of Chl-*a* anomalies appear~~are~~ spotty, with average positive and negative Chl-*a* anomalies in AEs and CEs, respectively. The amplitude and Chl-*a* anomalies are negatively correlated in subtropical waters north of the ACC and positively correlated along the ACC.

The distributions of DIC anomalies differ significantly~~greatly~~ from ~~that~~ those of SST and Chl-*a* anomalies, with uniform speckles featuring average negative ~~(positive)~~ DIC anomalies in WAEs and WCEs and positive DIC anomalies in ~~(~~CAEs and CCEs~~)~~ (Figs. 3~~6~~i–l). In addition to the opposite DIC anomaly signals between normal and ~~abnormal~~"abnormal" eddies, the magnitudes of DIC ~~anomaly~~ anomalies are generally larger in ~~magnitudes of~~ normal eddies ~~are larger~~ than in ~~abnormal~~"abnormal" eddies.

The patterns of eddy-induced pCO_2 anomalies are zonal. For AEs ~~(CEs)~~, ~~the~~ pCO_2 anomalies are positive ~~(negative)~~ in the north of ACC and negative ~~(positive)~~ along the ACC, while the opposite is true for CEs (Figs. 3~~6~~m–p). However, there are some distinctions between normal and ~~abnormal~~"abnormal" eddies. For example, in the north of ACC (including SWA) with high SST and low DIC (Figs. 4~~7~~a1, b1), WAEs ~~(~~and WCEs~~)~~ have more positive speckles compared to CAEs ~~(~~and CCEs~~)~~, respectively. Conversely~~In contrast~~, along the ACC (including ARC) with low SST and high DIC (Figs. 4~~7~~a1, b1), WAEs ~~(~~and WCEs~~)~~ have more negative speckles ~~compared to~~than CAEs ~~(~~and CCEs~~)~~.

These findings indicate variability in the spatial distribution of physical and ~~biochemical~~biogeochemical parameters ~~induced~~caused by normal and ~~abnormal~~"abnormal" eddies. To further quantify the effects of eddies on different parameters, we average all eddy-centric composite maps for SST, Chl-*a*, DIC, and pCO_2 anomalies over eddies to analyze the pattern characteristics of eddy-induced parameters. Due to seasonal variations in pCO_2, eddies' physical and ~~biochemical~~biogeochemical characteristics are also synthesized in summer and winter.

4.3 Composite Maps of Eddy-induced SST, Chl-*a*, DIC, pCO_2 Anomalies

Using the eddy-centric composite method (Fig. S2~~3~~), we investigate~~d~~ the seasonal variations of SST, Chl-*a*, DIC, and pCO_2 associated with normal and ~~abnormal~~"abnormal" eddies in the SO (Fig. 5~~8~~). Figures 5~~8~~a1–a4 and e1–e4 show the composite SST anomalies within normal and ~~abnormal~~"abnormal" eddies in winter and summer, respectively. There are no significant differences in the signals and spatial patterns of SST anomalies within the same kind of eddies ~~in~~ between summer and winter. Composite SST anomalies over normal eddies show asymmetric monopole patterns, with positive ~~(~~/negative~~)~~ extremums slightly shifting westward and poleward (equatorward) relative to the WAEs ~~(~~/CCEs~~)~~ cores. In comparison, ~~abnormal~~"abnormal" eddies also display monopole patterns but with opposite signals. Furthermore~~Besides~~, the magnitudes of SST anomalies over normal eddies are larger than those over ~~abnormal~~"abnormal" eddies.

The composite Chl-*a* anomalies within the same kind of eddies also show~~have~~ no obvious seasonality in the signals and spatial patterns (Figs. 5~~8~~b1–b4 and f1–f4). Moreover, composite Chl-*a* anomalies have no significant difference between normal and ~~abnormal~~"abnormal" eddies, with monopole negative ~~(positive)~~ signals in WAEs and CAEs and positive signals in ~~(~~CCEs and WCEs~~)~~. ~~Besides, t~~The extremums of Chl-*a* anomalies slightly shift poleward ~~(equatorward)~~ relative to the cores of WAEs and CAEs and equatorward relative to the cores of ~~(~~CCEs and WCEs~~)~~.

Regarding eddy-induced DIC anomalies, their composite maps within the same kind of eddies are similar in summer and winter, except that the magnitudes of DIC anomalies within eddies are slightly higher in winter (Figs. 5~~8~~c1–c4 and g1–g4). Moreover, the composite DIC anomalies within normal and ~~abnormal~~"abnormal" eddies show dipole patterns dominated by opposite signals. WAEs ~~(CCEs)~~ are dominated by negative ~~(positive)~~ DIC anomalies, whereas CAEs are dominated by positive DIC anomalies~~, . but CAEs (WCEs) are dominated by positive (negative) DIC anomalies, in contrast to SST signals.~~ CCEs are dominated by positive DIC anomalies, whereas WCEs are dominated by negative DIC anomalies. The DIC anomalies have opposite signals to SST anomalies within the same kind of eddies.

Although pCO_2 is influenced by SST, Chl-*a*, and DIC, pCO_2 anomalies within eddies in winter are significantly different from summer, unlike SST, Chl-*a*, and DIC anomalies within eddies similar in summer and winter (Figs. 58d1–d4 and h1–h4). To determine which factor dominates the change in pCO_2, ~~To quantify the similarity of the patterns between the pCO_2 and other anomalies over eddies,~~ we calculate~~d~~ the structural similarity index (SSIM) in Eq. (5), which can quantify the similarity of the patterns between pCO_2 and other anomalies over eddies (Wang et al., 2004).

$$SSIM\ (X,Y) = \frac{(2\mu_X\mu_Y + D_1)(2\sigma_{XY} + D_2)}{(\mu_X^2+\mu_Y^2+D_1)(\sigma_X^2+\sigma_Y^2+D_2)}$$
$$D_1 = (k_1 L_p)^2 \qquad (5)$$
$$D_2 = (k_2 L_p)^2$$

where X and Y denote composite averages of normalized pCO_2 and DIC (SST) anomalies, respectively. μ_X and μ_Y are the average values of X and Y. σ_X and σ_Y are the standard deviations of X and Y. σ_{XY} is the covariance of X and Y. L_p is the dynamic range of values, $L_p = 2$. k_1=0.01 and k_2=0.03. SSIM ranges from ~~–~~1 to 1. The closer the SSIM value is to 1, the more similar the two patterns are. Because the Chl-*a* negatively correlates~~is negatively correlated~~ with the pCO_2, its SSIMs are multiplied by −1. In winter, the SSIMs between pCO_2 and DIC anomalies are the largest (>0.9). The pCO_2 anomalies have similar patterns and signals with DIC anomalies, dominant by positive signals within CAEs and CCEs and negative signals within WAEs and WCEs (Figs. 58d1–d4). However, in summer, the SSIMs are negative between pCO_2 and DIC anomalies but positive between pCO_2 and SST (Chl-*a*) anomalies over eddies in summer (≤ 0.35). The patterns of pCO_2 anomalies differ from those of SST, Chl-*a*, and DIC within eddies in the SO (Figs. 58h1–h4).

5 Modulation Mechanisms of Normal and ~~Abnormal~~"Abnormal" Eddies to Physical and ~~Biochemical~~Biogeochemical Parameters

This section discusses how eddies affect SST, Chl-*a*, DIC, and pCO_2 through various mechanisms, including eddy stirring, trapping, pumping, and eddy-induced Ekman pumping (Fig. 69).

5.1 Mechanism Analysis of Eddy's Influence on SST

Composite SST anomalies over eddies show monopole patterns, with positive anomalies ~~(negative)~~ in WAEs and WCEs and negative anomalies in ~~(~~CCEs and CAEs~~)~~ (Figs. 58a1–a4 and e1–e4). First, we analyze the effect of eddy trapping on SST, which is determined by the directions of horizontal SST gradient and eddy propagation (Frenger et al., 2015; Frenger et al., 2018). The climatological~~climatology~~ and seasonal averages of SST reveal a~~show that the SST is~~ zonal~~ly~~ ~~distributed~~ distribution with ~~and~~ a southward decrease~~s southward~~ (Figs. 47a1–a3). The tracks of long-lived eddies with lifetimes longer than 1 year~~–~~ indicate that the predominant~~show that the major~~ propagation direction of eddies is westward, with AEs propagating north and CEs propagating south (Fig. 710). According~~Due~~ to the southward decreasing SST, northward ~~(southward)~~ propagating WAEs ~~(CCEs)~~ would trap cold ~~(warm)~~ water and result in~~cause~~ negative ~~(positive)~~ SST anomalies.

Conversely, southward propagating CCEs would trap warm water and lead to positive SST anomalies. However, t~~T~~his process contradicts the observed~~actual~~ results, indicating that~~so we exclude~~ the effect of eddy trapping on SST can be excluded.

~~Besides, t~~The meridional and zonal phase shifts in normal eddies are proposed to be induced by the large-scale background SST gradient and eddy stirring. WAEs rotating counterclockwise through the SST gradient would advect warmer water from the north to the southeast. Conversely, CCEs rotating clockwise through the SST gradient would advect cooler water from the south to the northwest. In summary, for the advective effects of eddies, the effect of eddy trapping on SST is not reflected, and eddy stirring contributes to~~affects~~ the slight shift of SST anomalies extremums within normal eddies.

For the vertical effects of eddies, eddy pumping within AEs ~~(CEs)~~ associated with downwelling ~~(upwelling)~~ induces positive ~~(negative)~~ SST anomalies, while eddy pumping within CEs associated with upwelling induces negative SST anomalies (Fig. 6c). On the other hand, eddy-induced Ekman pumping within AEs ~~(CEs)~~ associated with upwelling ~~(downwelling)~~ induces negative ~~(positive)~~ SST anomalies, while eddy-induced Ekman pumping within CEs associated with downwelling induces positive SST anomalies (Fig~~s~~. 6~~9c,~~ d) (Gaube et al., 2013; Dawson et al., 2018). These~~Such~~ processes are consistent with the observed patterns of eddy-induced SST anomalies ~~we found~~. Moreover~~Furthermore~~, ~~we found that~~ WAEs/CCEs have stronger~~greater~~ positive/negative SST anomalies in the regions with larger amplitude, while CAEs/WCEs have weaker negative/positive SST anomalies (Figs. 3~~6~~a–d). The observation suggests~~is result reflects~~ that the strength of eddy pumping is positively correlated with eddy amplitude, i.e., ~~greater~~ larger amplitude corresponds to~~means~~ stronger downwelling and upwelling in the cores of AEs and CEs, respectively. Table S1 shows that the amplitudes of ~~abnormal~~"abnormal" eddies are smaller than normal eddies, indicating weaker~~, which means~~ eddy pumping ~~of~~ in ~~abnormal~~"abnormal" eddies ~~is weaker than normal eddies~~. Hence, ~~abnormal~~"abnormal" eddies are more likely to be influenced by eddy-induced Ekman pumping. In summary~~conclusion~~, within normal eddies, eddy pumping dominates the vertical heat advection, resulting in positive SST anomalies in WAEs ~~(~~and negative~~)~~ SST anomalies in ~~SST anomalies in WAEs (~~CCEs~~)~~ (Figs. 5~~8~~a1, a3, e1, and e3). However, within ~~abnormal~~"abnormal" eddies, the effect of eddy-induced Ekman pumping becomes more prominent~~overcomes the effect of eddy pumping~~, resulting in negative ~~(positive)~~ SST anomalies in CAEs ~~(~~and positive SST anomalies in WCEs~~)~~ (Figs. 5~~8~~a2, a4, e2, and e4).

5.2 Mechanism Analysis of Eddy's Influence on Chl-*a*

The composite maps of eddy-induced Chl-*a* anomalies in the SO show asymmetric monopole patterns, with negative ~~(~~/positive~~)~~ extremums shifting poleward ~~(~~/equatorward~~)~~ relative to the AEs ~~(~~/CEs~~)~~ cores (Figs. 5~~8~~b1–b4 and f1–f4). We calculate the climatological average gradient of Chl-*a* in the SO from 1996 to 2015, which is normalized before calculation. The north-south gradient of Chl-*a* is −0.02 (north is the positive direction), while the east-west gradient of Chl-*a* is −0.04 (east is the positive direction). Due to the climatological Chl-*a* increasing southward (Figs. 4~~7~~b1–b3), ~~AEs (CEs) propagating northward (southward) would trap high (low) Chl-*a*, contrary to the composite Chl-*a* anomalies over eddies.~~

带格式的: 缩进：首行缩进：1 字符

AEs propagating northward tend to trap high Chl-*a* into northern areas with low Chl-*a*. Conversely, CEs propagating southward tend to trap low Chl-*a* into southern areas with high Chl-*a*. However, this effect of eddy trapping on Chl-*a* contradicts the actual composite Chl-*a* anomalies over eddies with negative Chl-*a* anomalies in AEs and positive Chl-*a* anomalies in CEs (Figs. 5~~8~~b1–b4 and f1–f4). Therefore, eddy trapping has little influence on Chl-*a*.

Moreover, considering that the climatological Chl-*a* increases southward and westward, the counterclockwise rotation of AEs in the SO would advect low Chl-*a* from the northeast to the west and high Chl-*a* from the southwest to the east. The reverse is true for CEs. Previous works found that the dipole shapes arising from stirring tend to be asymmetric, with larger anomalies on the leading side compared to the trailing side of eddies (Chelton et al., 2011b; Frenger et al., 2015; Dawson et al., 2018; Frenger et al., 2018). As the major propagation direction of eddies is westward (Fig. 7~~10~~), the composite Chl-*a* anomalies in AEs/CEs show dominant negative/positive signals due to eddy stirring.~~However, eddy stirring contributes to the meridional shifts of Chl-*a* anomalies in eddies. Under the southward increasing Chl-*a*, counterclockwise rotation of AEs advects low Chl-*a* from the north to the southeast and high Chl-*a* from the south to the northwest. The reverse is true for CEs. Previous works find~~ found that the dipole shapes arising from stirring tend to be asymmetric, with larger anomalies at the leading compared to the trailing side of eddies (Chelton et al., 2011; Frenger et al., 2015; Dawson et al., 2018; Frenger et al., 2018). Such patterns induced by eddy stirring are consistent with the summer composite maps of Chl-*a* anomalies (Figs. 8f1–f4) but less consistent with the winter ones (Figs. 8b1–b4), which is related to the smaller Chl-*a* gradient in winter than in summer (Figs. 7b2 and b3).

Eddy pumping induces negative ~~(~~and positive~~)~~ Chl-*a* anomalies within AEs ~~(~~and CEs~~)~~, respectively, ~~while~~ on the contrary, eddy-induced Ekman pumping induces positive ~~(~~and negative~~)~~ Chl-*a* anomalies within AEs ~~(~~and CEs~~)~~, respectively (Dawson et al., 2018). The eddy-centric composite maps of Chl-*a* anomalies show monopole negative ~~(positive)~~ signals in AEs ~~(CEs)~~ and positive signals in CEs~~, suggesting the negligible effect of eddy-induced Ekman pumping on Chl-*a*~~ (Figs. 5~~8~~b1–b4 and f1–f4). Besides, in regions of higher amplitude, the magnitudes of eddy-induced Chl-*a* anomalies are greater (Figs. 3~~6~~e–h). ~~This~~ These result~~s~~ reflect~~s~~ the dominant effect of eddy pumping on Chl-*a* anomalies within eddies. From Figs. 5~~8~~b1–b4 and f1–f4, we can see that the magnitudes of Chl-*a* anomalies within normal eddies are higher than "abnormal" eddies, which reflects the effect of eddy-induced Ekman pumping. It is worth noting that in some regions with small amplitude, such as the south of ACC and the South Pacific Ocean, we observe positive Chl-*a* anomalies in AEs and negative Chl-*a* anomalies in CEs (Figs. 3~~6~~e–h). Such a result may be caused by a more dominant effect of eddy-induced Ekman pumping on Chl-*a*. ~~Therefore~~Overall, eddy stirring and eddy pumping are mainly responsible for the patterns of Chl-*a* anomalies within eddies in the SO, and eddy-induced Ekman pumping attenuates the magnitudes of Chl-*a* anomalies within "abnormal" eddies.

5.3 Mechanism Analysis of Eddy's Influence on DIC

The composite DIC anomalies within normal and ~~abnormal~~"abnormal" eddies show dipole patterns with opposite ~~dominated~~ dominant ~~by opposite~~ signals, negative ~~(positive)~~ in WAEs and WCEs ~~(~~and positive in CAEs and CCEs~~)~~ in the SO (Figs. 5~~8~~c1–c4 and g1–g4). The dipole patterns are affected by eddy stirring. ~~For example, u~~Under the condition of southward

带格式的: 缩进：首行缩进：1 字符

increasing DIC (Figs. 47c1–c3), AEs ~~(CEs)~~ propagating northward ~~(southward)~~ tend to~~would~~ trap high ~~(low)~~ DIC, whereas CEs propagating southward tend to trap low DIC. Thus, the effect of eddy trapping may contribute to the positive and negative signals of DIC anomalies within AEs and CEs, respectively. However, ~~the advective effects of eddies cannot explain~~ the opposite dominant signals between normal and ~~abnormal~~"abnormal" eddies cannot be explained solely by the advective effects of eddies.

Eddy pumping induces negative DIC anomalies within AEs through the downwelling of surface low-DIC waters and positive DIC anomalies within CEs through the upwelling of deep rich-DIC waters. The reverse is true for the effect of eddy-induced Ekman pumping on DIC anomalies. As mentioned in Section 5.1, the greater amplitude of eddies corresponds to~~means~~ stronger eddy pumping. The ~~greater~~ larger amplitude of normal eddies than ~~abnormal~~"abnormal" eddies leads to higher~~increases the~~ magnitudes of negative ~~(positive)~~ DIC anomalies ~~over~~ in WAEs ~~(CCEs)~~ and positive anomalies in CCEs. ~~Furthermore, the Ekman pumping caused by WAEs (WCEs) is stronger than that caused by CAEs (CCEs) (Figs. 11a1–a4), resulting in stronger positive (negative) DIC anomalies over WAEs (WCEs) than CAEs (CCEs).~~ Moreover, the Ekman pumping caused by WAEs is stronger than that caused by CAEs, resulting in stronger positive DIC anomalies within WAEs than CAEs. Similarly, the Ekman pumping caused by WCEs is stronger than that caused by CCEs, resulting in stronger negative DIC anomalies within WCEs than CCEs. Consequently, the ~~common~~ combined effects of eddy pumping and eddy-induced Ekman pumping contribute to~~result in~~ the dominant negative ~~(positive)~~ DIC anomalies within WAEs and WCEs and positive DIC anomalies within ~~(~~CAEs and CCEs~~)~~ in the SO.

5.4 Mechanism Analysis of Eddy's Influence on pCO_2

In winter, the pCO_2 anomalies have similar patterns and signals with DIC anomalies, and the SSIMs between pCO_2 and DIC anomalies are the highest in the SO (Figs. 58d1–d4), suggesting that the effect of DIC ~~effect~~ on pCO_2 is stronger than the effects of SST and Chl-*a* ~~effects~~. However, in summer, the patterns of pCO_2 anomalies differ significantly from the anomalies of SST, Chl-*a*, and DIC within eddies in the SO with relatively lower SSIMs (the highest SSIM~~s~~ is 0.35) (Figs. 58h1–h4). This result may be caused by different processes affecting pCO_2 in different regions of the SO. To prove this hypothesis, we further examine~~d~~ the eddy-induced SST, Chl-*a*, DIC, and pCO_2 anomalies in the SWA (95°–115°E, 30°–40°S) and ARC (25°–75°E, 35°–45°S), where the eddy activity is strong, and the eddy amplitude and rotation speed are high (Figs. 24, S35, magenta rectangular box), leading to strong eddy stirring, trapping and pumping (Dawson et al., 2018; Frenger et al., 2018). Moreover, we find that the eddy-induced Ekman pumping ~~of~~ within ~~abnormal~~"abnormal" eddies is stronger than normal eddies in the SWA, contrary to the ARC (Fig. 811).

Similar to the SO, the SSIMs between pCO_2 and DIC anomalies are the highest in both the SWA and ARC ~~in~~ during winter, indicating the dominant effect of DIC on pCO_2 (Figs. 912d1–d4 and 103d1–d4). However, unlike the SO, the SSIMs between pCO_2 and SST anomalies are the highest in the summer SWA (Figs. 912h1–h4). By contrast, the SSIMs between pCO_2 and DIC anomalies are the highest in summer ARC (Figs. 103h1–h4). These results suggest~~indicate~~ that in summer, the pCO_2 within eddies is dominated by the SST ~~(DIC)~~ effect in the SWA and dominated by the DIC effect in the ~~(~~ARC~~)~~.

~~Under the condition of~~ Despite similar magnitudes of SST anomalies over eddies between the SWA and ARC, the magnitudes of DIC anomalies in the SWA are significantly ~~less~~ lower than those in the ARC, which may cause different processes affecting pCO_2 in the~~se~~ two regions. Likewise, the pCO_2 anomalies over eddies are determined by the DIC anomalies in winter, which is also associated with the higher magnitudes of DIC anomalies in winter compared to~~than in~~ summer. Such regional and seasonal magnitudes variation of DIC anomalies are controlled by the complex interactions among~~coupling of~~ processes such as~~,~~ biological activity (production/remineralization), vertical mixing, and air-sea gas exchanges (Racapé et al., 2010).

We further calculate the contributions of eddies to pCO_2 (Table S2). On average, the contributions of ~~abnormal~~"abnormal" eddies to pCO_2 are smaller than those of normal eddies in the SO and ARC. Nevertheless, the contributions of ~~abnormal~~"abnormal" eddies to pCO_2 are higher than those of normal eddies in the SWA. These finding~~result~~s are associated with~~related to~~ the dominance of ~~abnormal~~"abnormal" eddies in the SWA, driven~~caused~~ by the stronger eddy-induced Ekman pumping ~~of~~ observed in ~~abnormal~~"abnormal" eddies, compared to the SO and ARC (Figs. 2~~4~~, 8~~11~~). Additionally,~~Besides,~~ the contributions of the ARC and SWA eddies to pCO_2 are higher than the SO eddies, which is caused by the regional cancellation effect in the SO (Figs. 3~~6~~m–p). In the SO and ARC, the contributions of eddies to pCO_2 ~~in winter~~ are higher in winter than in summer (except WCEs in ARC), with a maximum value~~s~~ of 2.64 % (WAEs in the SO) and 5.03 % (CCEs in the ARC). However, in the SWA, the contributions of eddies to pCO_2 in summer are higher than in winter, with a maximum value~~s~~ of 5.15 % in WCEs, which is about 2.7 times higher than that of CCE. In summary~~conclusion~~, the contribution~~s~~ of eddies to pCO_2 ~~varies~~ vary depending on the~~by~~ eddy type, region, and season.

6 Discussion and Conclusions

~~Using the eddy-centric composite method, we investigated the effects of normal and abnormal eddies in modulating the variability of SST, Chl-*a*, DIC, and pCO_2 in the SO from 1996 to 2015. First, we analyzed the advective effects of eddies, including eddy trapping and stirring, based on variables gradient direction and eddy migration direction. Then, based on the eddy amplitude and the calculated W'_{ek}, we analyzed the vertical pumping effects of eddies, including eddy pumping and eddy-induced Ekman pumping.~~Section 5 reveals distinct influence mechanisms of eddies on SST, Chl-*a*, DIC, and pCO_2, which vary based on the inherent properties of each parameter and the complex interactions between eddies and the biogeochemical processes in the SO. As shown in Table 1, we compare the significance magnitudes of different effects, including eddy trapping, stirring, pumping, and eddy-induced Ekman pumping, on SST, Chl-*a*, and DIC. It should be noted that the seasonal modulation of the mixed layer is not discussed in our study due to the absence of significant seasonal variations in eddy-induced SST, Chl-*a*, and DIC anomalies (Figure S5). Additionally, the variability of pCO_2 anomalies within eddies is controlled by the effects of SST, Chl-*a*, and DIC, therefore, the eddy-driven mechanisms on pCO_2 can be demonstrated by exploring the effects of eddies on SST, Chl-*a*, and DIC.

Compared to SST, eddy stirring plays a more significant role in Chl-*a* and DIC anomalies within eddies. As eddy stirring redistributes physical and biogeochemical parameters spatially through horizontal advection, the larger the horizontal parameter gradient, the stronger the eddy stirring effect (Mcgillicuddy, 2016). We calculate the average gradients of normalized SST, Chl-*a*, and DIC in the SO from 1996 to 2015 and find their values are 0.05, 0.11, and 0.20, respectively. The specific method to obtain the gradients is demonstrated in Text S1 (Quarteroni et al., 2006). The small gradient of SST leads to a negligible effect of eddy stirring and results in more pronounced monopole patterns within eddies than other variables (Figs. 5a1–a4 and e1–e4).

By contrast, the average gradient of Chl-*a* is nearly two times higher than that of SST, thus, eddy stirring can cause a stronger effect on Chl-*a*. Both eddy stirring and eddy pumping contribute to the generation of negative/positive Chl-*a* anomalies within AEs/CEs. The combined effects of eddy stirring and eddy pumping dominate the similar patterns of Chl-*a* anomalies in normal and "abnormal" eddies. However, the effect of eddy-induced Ekman pumping on Chl-*a* is relatively small and contributes to attenuating the magnitudes of Chl-*a* anomalies within "abnormal" eddies (Figs. 5b1–b4 and f1–f4).

Such limited influence of eddy-induced Ekman pumping on Chl-*a* in the SO was also reported by Gaube et al. (2014), who plotted global maps of the cross correlation of Chl-*a* anomalies and SSH, as well as eddy-induced Ekman pumping, revealing a negative correlation between Chl-*a* anomalies and SSH and a negative correlation between Chl-*a* anomalies and eddy-induce Ekman pumping in most areas of the SO. These results indicate that AEs have negative Chl-*a* anomalies and CEs have positive Chl-*a* anomalies, and eddy-induced Ekman pumping does not dominate the variation of Chl-*a* anomalies within eddies. In addition, we obtain the composite averages for Chl-*a* anomalies in the BMC, defined by Gaube et al. (2014) as 305°–330°E and 34°–50°S (Figure S4). The patterns are similar to those obtained by Gaube et al. (2014), with dominant monopole negative Chl-*a* anomalies within AEs and positive Chl-*a* anomalies within CEs. However, we find the magnitudes of Chl-*a* anomalies within "abnormal" eddies are smaller than normal eddies, which associates with the effect of eddy-induce Ekman pumping.

The average gradient of DIC is four times higher than that of SST, indicating that eddy stirring will have a more pronounced impact on DIC than on SST. As a result, the composite DIC anomalies within eddies show dipole patterns (Figs. 5c1–c4 and g1–g4). In addition to the different impacts of eddy stirring on SST and DIC, both eddy pumping and eddy-induced Ekman pumping contribute to the variations in these parameters (Table 1). In normal eddies, eddy pumping dominates the vertical distribution of SST and DIC. Within CCEs, the upwelling of cold, DIC-rich deep water induces negative SST anomalies and positive DIC anomalies, whereas the reverse is true for WAEs. However, the influence of eddy-induced Ekman pumping becomes more prominent within "abnormal" eddies. Within WCEs, the downwelling of warm, low-DIC surface waters induces positive SST anomalies and negative DIC anomalies, whereas the reverse is true for CAEs.

~~For eddy-induced SST anomalies, eddy pumping contributes to the positive/negative SST anomalies in WAEs/CCEs, and eddy-induced Ekman pumping contributes to the negative/positive SST anomalies in CAEs/WCEs. Eddy stirring and eddy pumping are the main modulation processes of normal and abnormal eddies to Chl-*a* in the SO. Composite Chl-*a* anomalies display negative (positive) signatures in both WAEs and CAEs (CCEs and WCEs). Caused by eddy stirring, composite DIC~~

~~anomalies show dipole patterns in both normal and abnormal eddies. Furthermore, composite DIC anomalies are dominant by negative/positive signatures in WAEs/CCEs due to eddy pumping, in contrast to that in CAEs/WCEs caused by eddy-induced Ekman pumping. There are no significant seasonal variations in eddy-induced SST, Chl-*a*, and DIC anomalies, contrary to eddy-induced pCO_2 anomalies that vary by season and region~~The impact of eddies on pCO_2 anomalies varies by season and region, which arises from the combined effects of SST, Chl-*a*, and DIC. In winter, the dominant DIC-driven effect leads to negative pCO_2 anomalies in WAEs and WCEs, and positive anomalies in CAEs and CCEs. ~~the pCO_2 anomalies are negative (positive) in WAEs and WCEs (CAEs and CCEs) caused by the dominant DIC-driven effect.~~ However, in summer, the pCO_2 anomalies are dominated by the ~~common~~ combined effects of SST, Chl-*a*, and DIC. Notably~~Moreover~~, the pCO_2 anomalies within eddies are dominated by DIC ~~(SST)~~ anomalies in the ARC ~~(SWA)~~, with larger ~~(smaller)~~ magnitudes of DIC anomalies in summer. In contrast, the pCO_2 anomalies within eddies are dominated by SST anomalies in the SWA, with smaller magnitudes of DIC anomalies.

In conclusion, using the eddy-centric composite method, we investigate the effects of normal and "abnormal" eddies on the variability of SST, Chl-*a*, DIC, and pCO_2 in the SO from 1996 to 2015. The modification of ~~abnormal~~"abnormal" eddies to physical and ~~biochemical~~biogeochemical parameters differs from normal eddies due to the combined~~common~~ effects of eddy pumping and eddy-induced Ekman pumping. In the SWA dominated by ~~abnormal~~"abnormal" eddies, the contributions of ~~abnormal~~"abnormal" eddies to pCO_2 are opposite to normal eddies and are about twice as high as normal eddies. The current research commonly combines all the AEs or CEs and masks the presence of CAEs and WCEs with very different upper ocean properties. Given their abundance, ~~we~~ considering~~consider~~ the role of ~~abnormal~~"abnormal" eddies when investigating eddy-induced modulation in physical and biogeochemical parameters~~air-sea variables~~, provides a more accurate estimation of the impact of mesoscale eddies ~~which helps to estimate mesoscale eddies' impact more accurately~~.

~~This work provides an~~The observational-based study of basin-wide surface physical and ~~biochemical~~biogeochemical parameters within~~in the~~ SO mesoscale eddies ~~and will help to improve parameterizing mesoscale processes in models used to simulate and predict ocean biogeochemistry and carbon uptake.~~ provides important insights into the SO ecosystem and carbon cycling. The spatial redistribution of Chl-*a* concentrations through eddy stirring and eddy pumping indicates the potential for localized hotspots of productivity and nutrient supply within eddies. Moreover, the impacts of eddy pumping and eddy-induced Ekman pumping on DIC distributions highlight the role of eddies in transporting carbon-rich waters, which can significantly influence the regional carbon budget and oceanic carbon uptake. Understanding the complexity of eddy-driven processes in the SO is crucial for accurately simulating and predicting the biogeochemical dynamics of the SO and its role in the global carbon cycle. Further investigations focusing on the specific mechanisms driving the observed patterns and their consequences for larger-scale oceanic processes will provide valuable insights into the role of mesoscale eddies in the SO.

Data availability

All data used in the analysis are available in public repositories. The OISST data is available from https://www.ncei.noaa.gov/data/sea-surface-temperature-optimum-interpolation/v2.1/access/avhrr/. The Chl-*a* product is available from https://data.marine.copernicus.eu/product/OCEANCOLOUR_GLO_BGC_L3_MY_009_103/services. The pCO_2 and DIC datasets are available from https://www.data.jma.go.jp/gmd/kaiyou/english/co2_flux/co2_flux_data_en.html. Normal and ~~abnormal~~"abnormal" eddies datasets are available from https://figshare.com/s/3c3b03776d9862ac85bc for peer review only. The CCMP vector wind data is available from https://www.remss.com. The AVISO altimeter current product is available from https://data.marine.copernicus.eu/product/SEALEVEL_GLO_PHY_L4_MY_008_047/services. The positions of the main ACC fronts (Polar Front and Subantarctic Front) are available from http://ctoh.legos.obs-mip.fr/data/southern-ocean-fronts-extraction-form.

Author contributions

QL, YL, and FL conceived the project. QL did the writing and original draft preparation. All authors provided feedback on the analysis and interpretation of results and contributed to reviewing and editing the manuscript. All authors have read and agreed to the published version of the manuscript.

Competing interests

The authors declare that they have no conflict of interest.

Acknowledgements

This work was supported by the Qingdao National Laboratory for Marine Science and Technology, the special fund of Shandong province (No. LSKJ202204302), the Natural Science Foundation of Shandong Province (ZR2020MD083), the National Natural Science Foundation of China (U2006211), the Strategic Priority Research Program of the Chinese Academy of Sciences (XDA19060101, and XDB42000000), Major scientific and technological innovation projects of Shandong Province (2019JZZY010102), and the CAS Program (Y9KY04101L).

References

Altabet, M. A., Ryabenko, E., Stramma, L., Wallace, D. W. R., Frank, M., Grasse, P., and Lavik, G.: An eddy-stimulated hotspot for fixed nitrogen-loss from the Peru oxygen minimum zone, Biogeosciences, 9, 4897-4908, https://doi.org/10.5194/bg-9-4897-2012, 2012.

Assassi, C., Morel, Y., Vandermeirsch, F., Chaigneau, A., Pegliasco, C., Morrow, R., Colas, F., Fleury, S., Carton, X., Klein, P., and Cambra, R.: An Index to Distinguish Surface- and Subsurface-Intensified Vortices from Surface Observations, J. Phys. Oceanogr., 46, 2529-2552, https://doi.org/10.1175/jpo-d-15-0122.1, 2016.

Bakker, D. C. E., Pfeil, B., Landa, C. S., Metzl, N., O'Brien, K. M., Olsen, A., Smith, K., Cosca, C., Harasawa, S., Jones, S. D., Nakaoka, S., Nojiri, Y., Schuster, U., Steinhoff, T., Sweeney, C., Takahashi, T., Tilbrook, B., Wada, C., Wanninkhof, R., Alin, S. R., Balestrini, C. F., Barbero, L., Bates, N. R., Bianchi, A. A., Bonou, F., Boutin, J., Bozec, Y., Burger, E. F., Cai, W. J., Castle, R. D., Chen, L., Chierici, M., Currie, K., Evans, W., Featherstone, C., Feely, R. A., Fransson, A., Goyet, C., Greenwood, N., Gregor, L., Hankin, S., Hardman-Mountford, N. J., Harlay, J., Hauck, J., Hoppema, M., Humphreys, M. P., Hunt, C. W., Huss, B., Ibánhez, J. S. P., Johannessen, T., Keeling, R., Kitidis, V., Körtzinger, A., Kozyr, A., Krasakopoulou, E., Kuwata, A., Landschützer, P., Lauvset, S. K., Lefèvre, N., Lo Monaco, C., Manke, A., Mathis, J. T., Merlivat, L., Millero, F. J., Monteiro, P. M. S., Munro, D. R., Murata, A., Newberger, T., Omar, A. M., Ono, T., Paterson, K., Pearce, D., Pierrot, D., Robbins, L. L., Saito, S., Salisbury, J., Schlitzer, R., Schneider, B., Schweitzer, R., Sieger, R., Skjelvan, I., Sullivan, K. F., Sutherland, S. C., Sutton, A. J., Tadokoro, K., Telszewski, M., Tuma, M., van Heuven, S. M. A. C., Vandemark, D., Ward, B., Watson, A. J., and Xu, S.: A multi-decade record of high-quality fCO_2 data in version 3 of the Surface Ocean CO_2 Atlas (SOCAT), Earth Syst. Sci. Data, 8, 383-413, https://doi.org/10.5194/essd-8-383-2016, 2016.

Butterworth, S.: On the theory of filter amplifiers, Wireless Engineer 193-195, 1930.

Campbell, J. W.: The lognormal distribution as a model for bio-optical variability in the sea, J. Geophys. Res.: Oceans, 100, 13237-13254, https://doi.org/10.1029/95JC00458, 1995.

Castellani, M.: Identification of eddies from sea surface temperature maps with neural networks, Int. J. Remote Sens., 27, 1601-1618, https://doi.org/10.1080/01431160500462170, 2006.

Chelton, D. B., Schlax, M. G., and Samelson, R. M.: Global observations of nonlinear mesoscale eddies, Prog. Oceanogr., 91, 167-216, https://doi.org/10.1016/j.pocean.2011.01.002, 2011a.

Chelton, D. B., Gaube, P., Schlax, M. G., Early, J. J., and Samelson, R. M.: The Influence of Nonlinear Mesoscale Eddies on Near-Surface Oceanic Chlorophyll, Science, 334, 328-332, https://doi.org/doi:10.1126/science.1208897, 2011b.

Chen, F., Cai, W.-J., Benitez-Nelson, C., and Wang, Y.: Sea surface pCO_2-SST relationships across a cold-core cyclonic eddy: Implications for understanding regional variability and air-sea gas exchange, Geophys. Res. Lett., 34, https://doi.org/10.1029/2006gl028058, 2007.

Dawson, H. R. S., Strutton, P. G., and Gaube, P.: The Unusual Surface Chlorophyll Signatures of Southern Ocean Eddies, J. Geophys. Res.: Oceans, 123, 6053-6069, https://doi.org/10.1029/2017JC013628, 2018.

Denvil-Sommer, A., Gehlen, M., Vrac, M., and Mejia, C.: LSCE-FFNN-v1: a two-step neural network model for the reconstruction of surface ocean pCO_2 over the global ocean, Geosci. Model Dev., 12, 2091-2105, https://doi.org/10.5194/gmd-12-2091-2019, 2019.

Dilmahamod, A. F., Aguiar-González, B., Penven, P., Reason, C. J. C., De Ruijter, W. P. M., Malan, N., and Hermes, J. C.: SIDDIES Corridor: A Major East-West Pathway of Long-Lived Surface and Subsurface Eddies Crossing the Subtropical South Indian Ocean, J. Geophys. Res.: Oceans, 123, 5406-5425, https://doi.org/10.1029/2018JC013828, 2018.

Dolz, J., Gopinath, K., Yuan, J., Lombaert, H., Desrosiers, C., and Ben Ayed, I.: HyperDense-Net: A Hyper-Densely Connected CNN for Multi-Modal Image Segmentation, IEEE Trans. Med. Imaging, 38, 1116-1126, https://doi.org/10.1109/TMI.2018.2878669, 2019.

Dong, C. M., McWilliams, J. C., Liu, Y., and Chen, D. K.: Global heat and salt transports by eddy movement, Nat. Commun., 5, https://doi.org/10.1038/ncomms4294, 2014.

Ducet, N., Le Traon, P. Y., and Reverdin, G.: Global high-resolution mapping of ocean circulation from TOPEX/Poseidon and ERS-1 and -2, J. Geophys. Res.: Oceans, 105, 19477-19498, https://doi.org/10.1029/2000JC900063, 2000.

Dufois, F., Hardman-Mountford, N. J., Greenwood, J., Richardson, A. J., Feng, M., Herbette, S., and Matear, R.: Impact of eddies on surface chlorophyll in the South Indian Ocean, J. Geophys. Res.: Oceans, 119, 8061-8077, https://doi.org/https://doi.org/10.1002/2014JC010164, 2014.

Everett, J. D., Baird, M. E., Oke, P. R., and Suthers, I. M.: An avenue of eddies: Quantifying the biophysical properties of mesoscale eddies in the Tasman Sea, Geophys. Res. Lett., 39, https://doi.org/10.1029/2012gl053091, 2012.

Faghmous, J. H., Frenger, I., Yao, Y., Warmka, R., Lindell, A., and Kumar, V.: A daily global mesoscale ocean eddy dataset from satellite altimetry, Sci. Data, 2, 150028, https://doi.org/10.1038/sdata.2015.28, 2015.

Falk, T., Mai, D., Bensch, R., Cicek, O., Abdulkadir, A., Marrakchi, Y., Bohm, A., Deubner, J., Jackel, Z., Seiwald, K., Dovzhenko, A., Tietz, O., Dal Bosco, C., Walsh, S., Saltukoglu, D., Tay, T. L., Prinz, M., Palme, K., Simons, M., Diester, I., Brox, T., and Ronneberger, O.: U-Net: deep learning for cell counting, detection, and morphometry, Nat. Methods, 16, 67-70, https://doi.org/10.1038/s41592-018-0261-2, 2019.

Fay, A. R., Lovenduski, N. S., McKinley, G. A., Munro, D. R., Sweeney, C., Gray, A. R., Landschützer, P., Stephens, B. B., Takahashi, T., and Williams, N.: Utilizing the Drake Passage Time-series to understand variability and change in subpolar Southern Ocean pCO_2, Biogeosciences, 15, 3841-3855, https://doi.org/10.5194/bg-15-3841-2018, 2018.

Frenger, I., Münnich, M., and Gruber, N.: Imprint of Southern Ocean mesoscale eddies on chlorophyll, Biogeosciences, 15, 4781-4798, https://doi.org/10.5194/bg-15-4781-2018, 2018.

Frenger, I., Gruber, N., Knutti, R., and Münnich, M.: Imprint of Southern Ocean eddies on winds, clouds and rainfall, Nat. Geosci., 6, 608-612, https://doi.org/10.1038/ngeo1863, 2013.

Frenger, I., Münnich, M., Gruber, N., and Knutti, R.: Southern Ocean eddy phenomenology, J. Geophys. Res.: Oceans, 120, 7413-7449, https://doi.org/10.1002/2015jc011047, 2015.

Garnesson, P., Mangin, A., Fanton d'Andon, O., Demaria, J., and Bretagnon, M.: The CMEMS GlobColour chlorophyll a product based on satellite observation: multi-sensor merging and flagging strategies, Ocean Sci., 15, 819-830, https://doi.org/10.5194/os-15-819-2019, 2019.

Gaube, P., Chelton, D. B., Strutton, P. G., and Behrenfeld, M. J.: Satellite observations of chlorophyll, phytoplankton biomass, and Ekman pumping in nonlinear mesoscale eddies, J. Geophys. Res.: Oceans, 118, 6349-6370, https://doi.org/10.1002/2013JC009027, 2013.

Gaube, P., Chelton, D. B., Samelson, R. M., Schlax, M. G., and O'Neill, L. W.: Satellite Observations of Mesoscale Eddy-Induced Ekman Pumping, J. Phys. Oceanogr., 45, 104-132, https://doi.org/10.1175/jpo-d-14-0032.1, 2015.

Gaube, P., McGillicuddy Jr., D. J., Chelton, D. B., Behrenfeld, M. J., and Strutton, P. G.: Regional variations in the influence of mesoscale eddies on near-surface chlorophyll, J. Geophys. Res.: Oceans, 119, 8195-8220, https://doi.org/10.1002/2014JC010111, 2014.

Gille, S. T., Carranza, M. M., Cambra, R., and Morrow, R.: Wind-induced upwelling in the Kerguelen Plateau region, Biogeosciences, 11, 6389-6400, https://doi.org/10.5194/bg-11-6389-2014, 2014.

Gohin, F., Druon, J. N., and Lampert, L.: A five channel chlorophyll concentration algorithm applied to SeaWiFS data processed by SeaDAS in coastal waters, Int. J. Remote Sens., 23, 1639-1661, https://doi.org/10.1080/01431160110071879, 2002.

Hashihama, F., Yasuda, I., Kumabe, A., Sato, M., Sasaoka, H., Iida, Y., Shiozaki, T., Saito, H., Kanda, J., Furuya, K., Boyd, P. W., and Ishii, M.: Nanomolar phosphate supply and its recycling drive net community production in the subtropical North Pacific, Nat. Commun., 12, 3462, https://doi.org/10.1038/s41467-021-23837-y, 2021.

Hausmann, U. and Czaja, A.: The observed signature of mesoscale eddies in sea surface temperature and the associated heat transport, Deep-Sea Research Part I-Oceanographic Research Papers 70, 60-72, https://doi.org/10.1016/j.dsr.2012.08.005, 2012.

Hu, C., Lee, Z., and Franz, B.: Chlorophyll aalgorithms for oligotrophic oceans: A novel approach based on three-band reflectance difference, J. Geophys. Res.: Oceans, 117, https://doi.org/10.1029/2011JC007395, 2012.

Huang, J., Xu, F., Zhou, K., Xiu, P., and Lin, Y.: Temporal evolution of near-surface chlorophyll over cyclonic eddy lifecycles in the southeastern Pacific, J. Geophys. Res.: Oceans, 122, 6165-6179, https://doi.org/10.1002/2017JC012915, 2017.

Iida, Y., Takatani, Y., Kojima, A., and Ishii, M.: Global trends of ocean CO_2 sink and ocean acidification: an observation-based reconstruction of surface ocean inorganic carbon variables, J. Oceanogr., 77, 323-358, https://doi.org/10.1007/s10872-020-00571-5, 2021.

Jersild, A. and Ito, T.: Physical and Biological Controls of the Drake Passage pCO_2 Variability, Global Biogeochem. Cycles, 34, https://doi.org/10.1029/2020gb006644, 2020.

Jones, E. M., Hoppema, M., Strass, V., Hauck, J., Salt, L., Ossebaar, S., Klaas, C., van Heuven, S. M. A. C., Wolf-Gladrow, D., Stöven, T., and de Baar, H. J. W.: Mesoscale features create hotspots of carbon uptake in the Antarctic Circumpolar Current, Deep Sea Res. Part II, 138, 39-51, https://doi.org/10.1016/j.dsr2.2015.10.006, 2017.

Landschützer, P., Gruber, N., Bakker, D. C. E., and Schuster, U.: Recent variability of the global ocean carbon sink, Global Biogeochem. Cycles, 28, 927-949, https://doi.org/10.1002/2014gb004853, 2014.

Landschützer, P., Gruber, N., Haumann, F. A., Rödenbeck, C., Bakker, D. C. E., Heuven, S. v., Hoppema, M., Metzl, N., Sweeney, C., Takahashi, T., Tilbrook, B., and Wanninkhof, R.: The reinvigoration of the Southern Ocean carbon sink, Science, 349, 1221-1224, https://doi.org/doi:10.1126/science.aab2620, 2015.

Lasternas, S., Piedeleu, M., Sangrà, P., Duarte, C. M., and Agustí, S.: Forcing of dissolved organic carbon release by phytoplankton by anticyclonic mesoscale eddies in the subtropical NE Atlantic Ocean, Biogeosciences, 10, 2129-2143, https://doi.org/10.5194/bg-10-2129-2013, 2013.

Le Quéré, C., Rödenbeck, C., Buitenhuis, E. T., Conway, T. J., Langenfelds, R., Gomez, A., Labuschagne, C., Ramonet, M., Nakazawa, T., Metzl, N., Gillett, N., and Heimann, M.: Saturation of the Southern Ocean CO_2 Sink Due to Recent Climate Change, Science, 316, 1735-1738, https://doi.org/doi:10.1126/science.1136188, 2007.

Leyba, I. M., Saraceno, M., and Solman, S. A.: Air-sea heat fluxes associated to mesoscale eddies in the Southwestern Atlantic Ocean and their dependence on different regional conditions, Clim. Dyn., 49, 2491-2501, https://doi.org/10.1007/s00382-016-3460-5, 2017.

Liu, Y., Yu, L., and Chen, G.: Characterization of Sea Surface Temperature and Air-Sea Heat Flux Anomalies Associated With Mesoscale Eddies in the South China Sea, J. Geophys. Res.: Oceans, 125, https://doi.org/10.1029/2019jc015470, 2020.

Liu, Y., Zheng, Q., and Li, X.: Characteristics of Global Ocean Abnormal Mesoscale Eddies Derived From the Fusion of Sea Surface Height and Temperature Data by Deep Learning, Geophys. Res. Lett., 48, https://doi.org/10.1029/2021gl094772, 2021.

Liu, Y., Chen, G., Sun, M., Liu, S., and Tian, F.: A Parallel SLA-Based Algorithm for Global Mesoscale Eddy Identification, J. Atmos. Oceanic Technol., 33, 2743-2754, https://doi.org/https://doi.org/10.1175/JTECH-D-16-0033.1, 2016.

Marshall, J. and Speer, K.: Closure of the meridional overturning circulation through Southern Ocean upwelling, Nat. Geosci., 5, 171-180, https://doi.org/10.1038/ngeo1391, 2012.

Mathis, J. T., Pickart, R. S., Hansell, D. A., Kadko, D., and Bates, N. R.: Eddy transport of organic carbon and nutrients from the Chukchi Shelf: Impact on the upper halocline of the western Arctic Ocean, J. Geophys. Res.: Oceans, 112, https://doi.org/10.1029/2006jc003899, 2007.

McGillicuddy, D. J.: Formation of Intrathermocline Lenses by Eddy–Wind Interaction, J. Phys. Oceanogr., 45, 606-612, https://doi.org/10.1175/jpo-d-14-0221.1, 2015.

McGillicuddy, D. J.: Mechanisms of Physical-Biological-Biogeochemical Interaction at the Oceanic Mesoscale, Annu. Rev. Mar. Science, 8, 125-159, https://doi.org/10.1146/annurev-marine-010814-015606, 2016.

McGillicuddy, D. J. and Robinson, A. R.: Eddy-induced nutrient supply and new production in the Sargasso Sea, Deep Sea Res. Part I, 44, 1427-1450, https://doi.org/10.1016/S0967-0637(97)00024-1, 1997.

McGillicuddy, D. J., Robinson, A. R., Siegel, D. A., Jannasch, H. W., Johnson, R., Dickey, T. D., McNeil, J., Michaels, A. F., and Knap, A. H.: Influence of mesoscale eddies on new production in the Sargasso Sea, Nature, 394, 263-266, https://doi.org/10.1038/28367, 1998.

McGillicuddy, D. J., Anderson, L. A., Bates, N. R., Bibby, T., Buesseler, K. O., Carlson, C. A., Davis, C. S., Ewart, C., Falkowski, P. G., Goldthwait, S. A., Hansell, D. A., Jenkins, W. J., Johnson, R., Kosnyrev, V. K., Ledwell, J. R., Li, Q. P., Siegel, D. A., and Steinberg, D. K.: Eddy/Wind Interactions Stimulate Extraordinary Mid-Ocean Plankton Blooms, Science, 316, 1021-1026, https://doi.org/doi:10.1126/science.1136256, 2007.

Melnichenko, O., Amores, A., Maximenko, N., Hacker, P., and Potemra, J.: Signature of mesoscale eddies in satellite sea surface salinity data, J. Geophys. Res.: Oceans, 122, 1416-1424, https://doi.org/10.1002/2016jc012420, 2017.

Nencioli, F., Chang, G., Twardowski, M., and Dickey, T. D.: Optical Characterization of an Eddy-induced Diatom Bloom West of the Island of Hawaii, Biogeosciences, 7, 151-162, https://doi.org/10.5194/bg-7-151-2010, 2010.

Ni, Q., Zhai, X., Jiang, X., and Chen, D.: Abundant Cold Anticyclonic Eddies and Warm Cyclonic Eddies in the Global Ocean, J. Phys. Oceanogr., 51, 2793-2806, https://doi.org/10.1175/jpo-d-21-0010.1, 2021.

Olsen, A., Lange, N., Key, R. M., Tanhua, T., Álvarez, M., Becker, S., Bittig, H. C., Carter, B. R., Cotrim da Cunha, L., Feely, R. A., van Heuven, S., Hoppema, M., Ishii, M., Jeansson, E., Jones, S. D., Jutterström, S., Karlsen, M. K., Kozyr, A., Lauvset, S. K., Lo Monaco, C., Murata, A., Pérez, F. F., Pfeil, B., Schirnick, C., Steinfeldt, R., Suzuki, T., Telszewski, M., Tilbrook, B., Velo, A., and Wanninkhof, R.: GLODAPv2.2019 – an update of GLODAPv2, Earth Syst. Sci. Data, 11, 1437-1461, https://doi.org/10.5194/essd-11-1437-2019, 2019.

Ono, H., Toyama, K., Enyo, K., Iida, Y., Sasano, D., Nakaoka, S.-I., and Ishii, M.: Meridional Variability in Multi-Decadal Trends of Dissolved Inorganic Carbon in Surface Seawater of the Western North Pacific Along the 165°E Line, J. Geophys. Res.: Oceans, 128, e2022JC018842, https://doi.org/https://doi.org/10.1029/2022JC018842, 2023.

Pegliasco, C., Delepoulle, A., Mason, E., Morrow, R., Faugère, Y., and Dibarboure, G.: META3.1exp: a new global mesoscale eddy trajectory atlas derived from altimetry, Earth Syst. Sci. Data, 14, 1087-1107, https://doi.org/10.5194/essd-14-1087-2022, 2022.

Pickart, R. S., Weingartner, T. J., Pratt, L. J., Zimmermann, S., and Torres, D. J.: Flow of winter-transformed Pacific water into the Western Arctic, Deep Sea Res. Part II, 52, 3175-3198, https://doi.org/10.1016/j.dsr2.2005.10.009, 2005.

Qiu, S., Feng, Y., Zhang, Y., Qi, D., Wu, Y., and Du, Y.: A Surface pCO_2 Increasing Hiatus in the Equatorial Pacific Ocean Since 2010, Geophys. Res. Lett., 48, e2021GL093612, https://doi.org/https://doi.org/10.1029/2021GL093612, 2021.

Quarteroni, A., Sacco, R., and Saleri, F.: Numerical Mathematics (Texts in Applied Mathematics), Springer-Verlag, 2006.

Racapé, V., Monaco, L., Metzl, N., and Pierre, C.: Summer and winter distribution of δ13CDIC in surface waters of the South Indian Ocean [20°S-60°S], Tellus B: Chem. Phys. Meteorol., 62, 660-673, https://doi.org/10.1111/j.1600-0889.2010.00504.x, 2010.

Reichstein, M., Camps-Valls, G., Stevens, B., Jung, M., Denzler, J., Carvalhais, N., and Prabhat: Deep learning and process understanding for data-driven Earth system science, Nature, 566, 195-204, https://doi.org/10.1038/s41586-019-0912-1, 2019.

Reynolds, R. W., Smith, T. M., Liu, C., Chelton, D. B., Casey, K. S., and Schlax, M. G.: Daily High-Resolution-Blended Analyses for Sea Surface Temperature, J. Clim., 20, 5473-5496, https://doi.org/10.1175/2007jcli1824.1, 2007.

Ronneberger, O., Fischer, P., and Brox, T.: U-Net: Convolutional Networks for Biomedical Image Segmentation, Medical Image Computing and Computer-Assisted Intervention – MICCAI 2015, 234-241, https://doi.org/10.48550/arXiv.1505.04597, 2015.

Sallée, J. B., Speer, K., and Morrow, R.: Response of the Antarctic Circumpolar Current to Atmospheric Variability, J. Clim., 21, 3020-3039, https://doi.org/10.1175/2007JCLI1702.1, 2008.

Shimizu, Y., Yasuda, I., and Ito, S.-i.: Distribution and Circulation of the Coastal Oyashio Intrusion, J. Phys. Oceanogr., 31, 1561-1578, https://doi.org/10.1175/1520-0485(2001)031<1561:Dacotc>2.0.Co;2, 2001.

Siegel, D. A., Peterson, P., McGillicuddy Jr., D. J., Maritorena, S., and Nelson, N. B.: Bio-optical footprints created by mesoscale eddies in the Sargasso Sea, Geophys. Res. Lett., 38, https://doi.org/10.1029/2011GL047660, 2011.

Song, H., Marshall, J., Munro, D. R., Dutkiewicz, S., Sweeney, C., McGillicuddy, D. J., and Hausmann, U.: Mesoscale modulation of air-sea CO_2 flux in Drake Passage, J. Geophys. Res.: Oceans, 121, 6635-6649, https://doi.org/10.1002/2016jc011714, 2016.

Stearns, S. D. and Ahmed, N.: Digital Signal Analysis, IEEE Transactions on Systems, Man, and Cybernetics, SMC-6, 724-724, https://doi.org/10.1109/TSMC.1976.4309433, 1976.

Stern, M. E.: Interaction of a uniform wind stress with a geostrophic vortex, Deep Sea Research and Oceanographic Abstracts, 12, 355-367, https://doi.org/https://doi.org/10.1016/0011-7471(65)90007-0, 1965.

Stramma, L., Bange, H. W., Czeschel, R., Lorenzo, A., and Frank, M.: On the role of mesoscale eddies for the biological productivity and biogeochemistry in the eastern tropical Pacific Ocean off Peru, Biogeosciences, 10, 7293-7306, https://doi.org/10.5194/bg-10-7293-2013, 2013.

Sun, W., Dong, C., Tan, W., and He, Y.: Statistical Characteristics of Cyclonic Warm-Core Eddies and Anticyclonic Cold-Core Eddies in the North Pacific Based on Remote Sensing Data, Remote Sens., 11, 208, 2019.

Villas Bôas, A. B., Sato, O. T., Chaigneau, A., and Castelão, G. P.: The signature of mesoscale eddies on the air-sea turbulent heat fluxes in the South Atlantic Ocean, Geophys. Res. Lett., 42, 1856-1862, https://doi.org/10.1002/2015gl063105, 2015.

Wang, Z., Bovik, A. C., Sheikh, H. R., and Simoncelli, E. P.: Image quality assessment: from error visibility to structural similarity, IEEE Trans. Image Process., 13, 600-612, https://doi.org/10.1109/TIP.2003.819861, 2004.

Xu, G., Dong, C., Liu, Y., Gaube, P., and Yang, J.: Chlorophyll Rings around Ocean Eddies in the North Pacific, Sci. Rep., 9, 2056, https://doi.org/10.1038/s41598-018-38457-8, 2019.

-Figures & tables

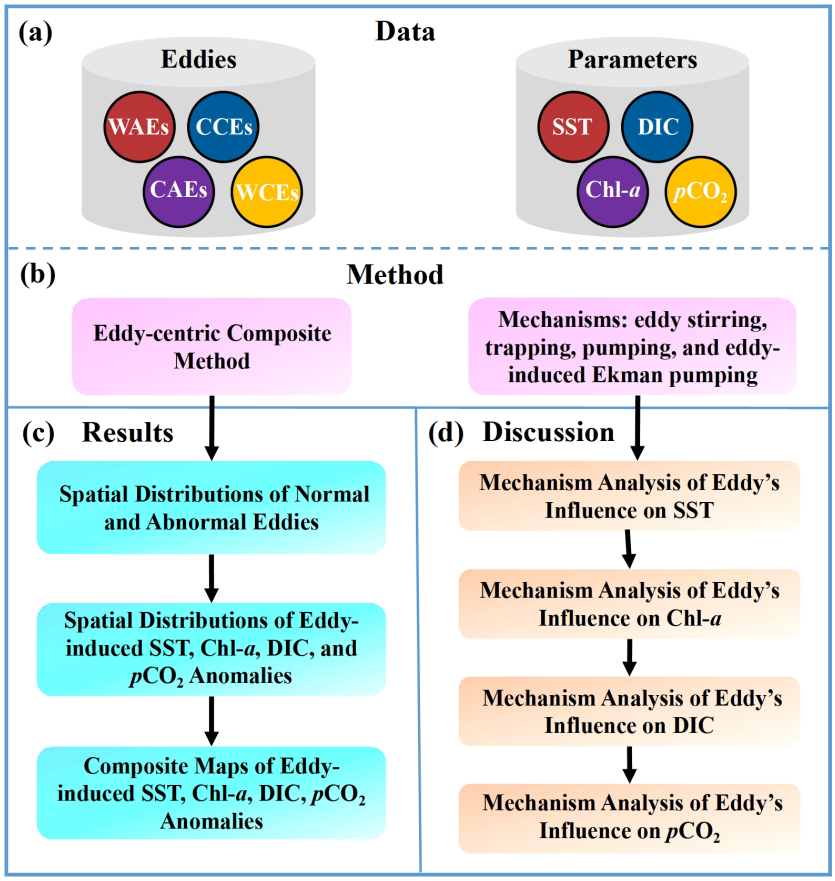

795 **Figure 1.** Research structure. Based on the eddy dataset, satellite SST and Chl-*a*, as well as observation-based reconstruction of DIC and pCO_2 from 1996 to 2015 in the SO, we use the eddy-centric composite method to conduct the composite patterns of SST, Chl-*a*, DIC, and pCO_2 associated with eddies. And then, we use mechanisms, including eddy stirring, trapping, pumping, and eddy-induced Ekman pumping, to analyze the modulation of eddies to SST, Chl-*a*, DIC, and pCO_2.

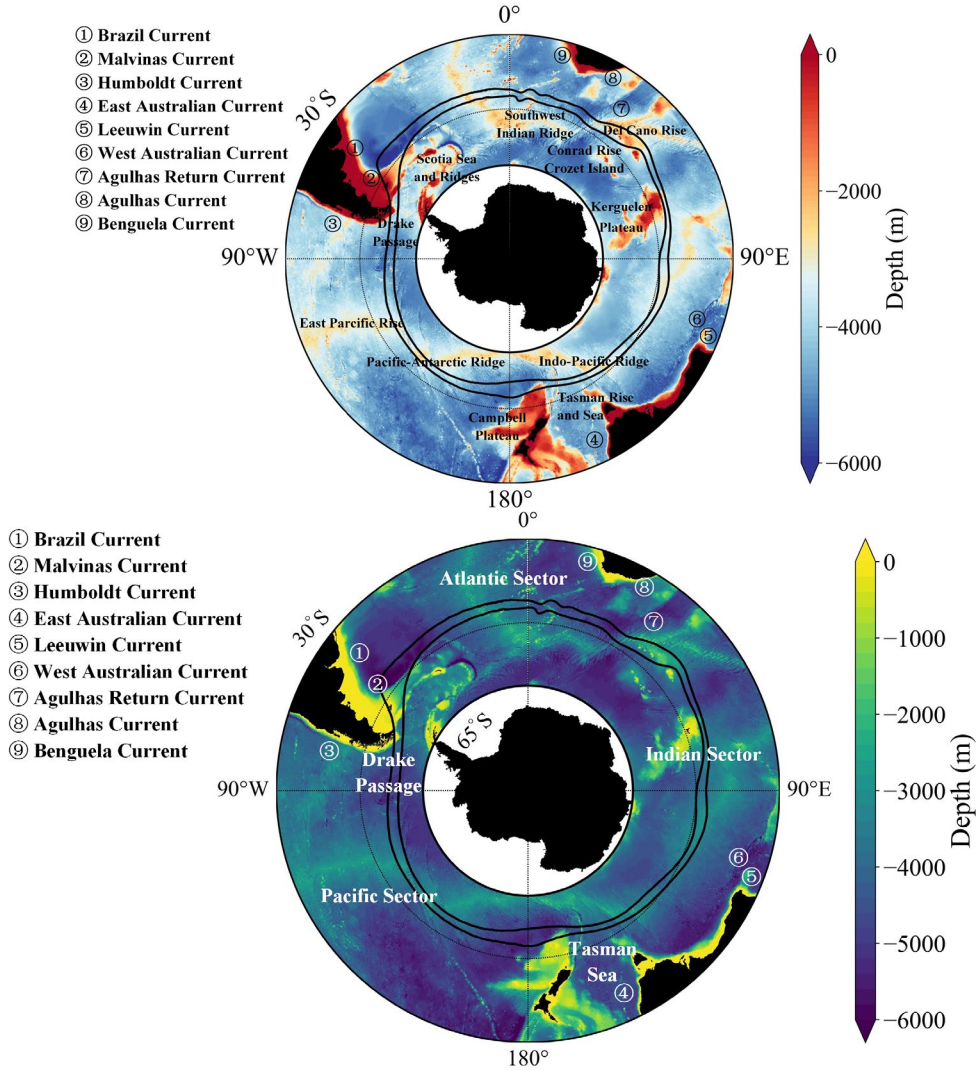

Figure 12. Southern Ocean topography and current. Black solid lines show the mean northern and southern positions of the ACC major fronts. The black dotted circle is 50° S.

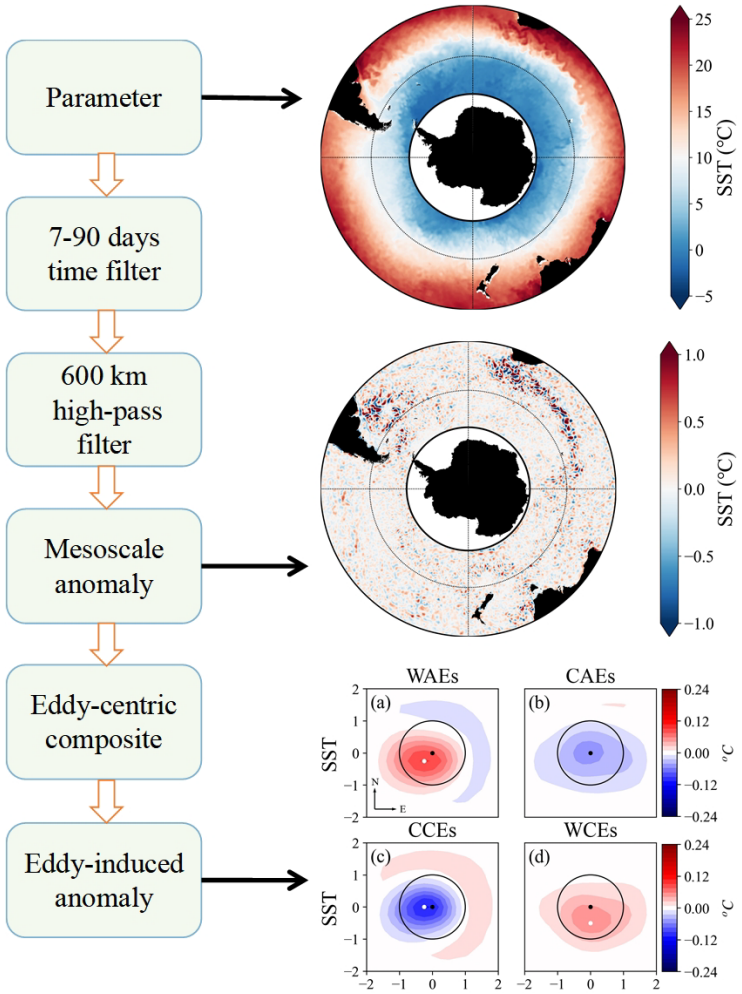

~~**Figure 3.** Schematic of eddy-centric composite method. The left column is the method structure. The right column is the result of the corresponding processing, taking SST as an example.~~

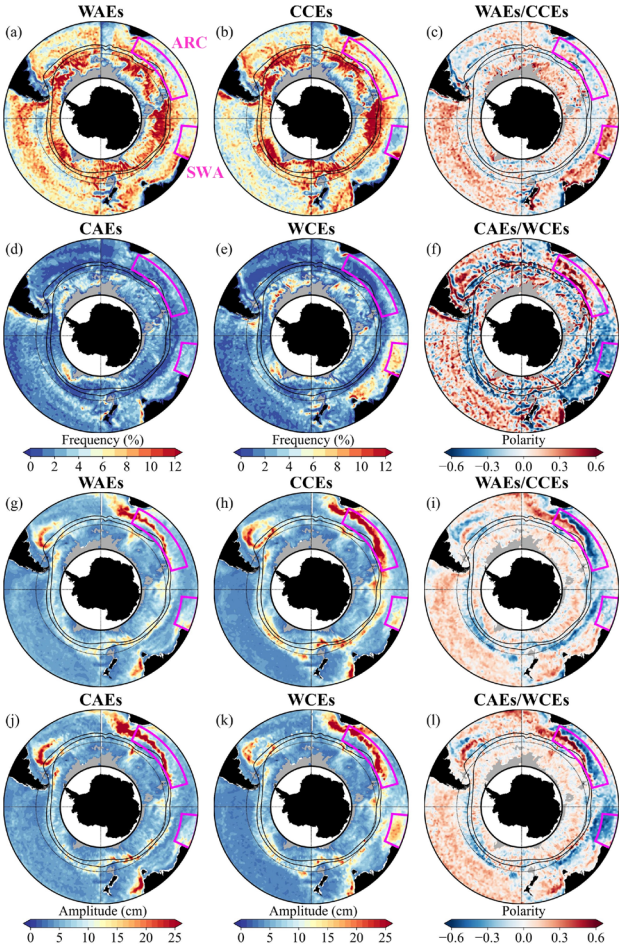

Figure 24. Spatial distribution of (a, b, d, and e) eddy frequency, (g, h, j, and k) eddy amplitude, and eddy polarity dominance in the SO from 1996 to 2015. (c, f) Ratio of the area occupied by WAEs ~~(~~/CAEs) over the area covered by CCEs ~~(~~/WCEs). (i, l) Ratio of amplitude for WAEs ~~(~~/CAEs) over CCEs ~~(~~/WCEs). For (c, f, i, l) eddy polarity, v~~V~~alues >0 in red and <0 in blue mark the dominance of AEs and CEs, respectively. Black solid lines show the mean northern and southern positions of the ACC major fronts. The black dotted circle is 50° S. The magenta boxes represent ARC and SWA regions.

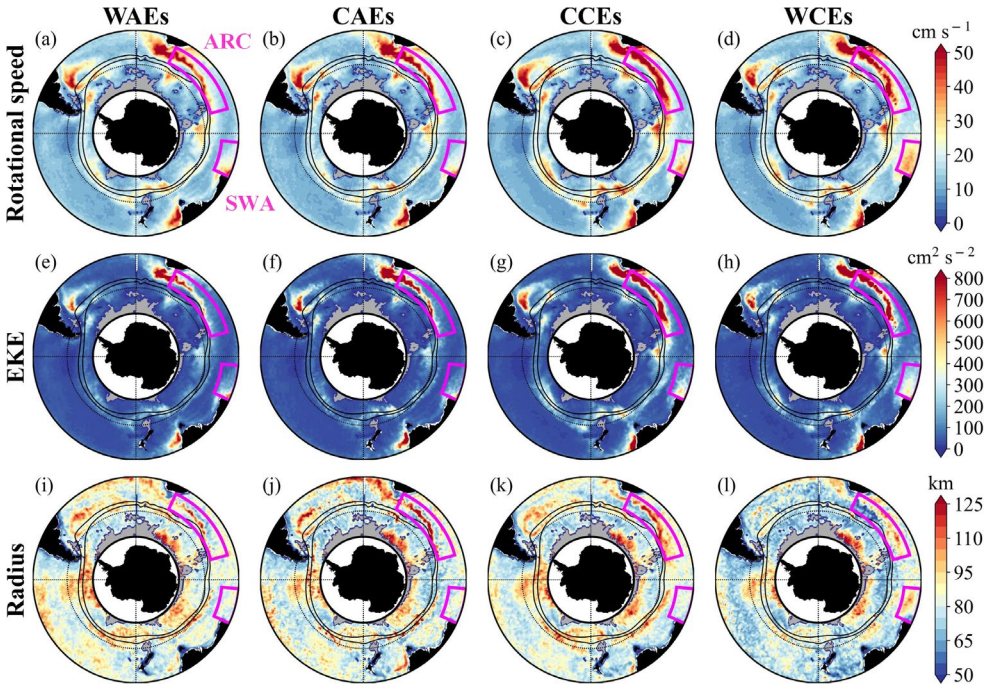

Figure 5. Spatial distribution of eddy properties, including (a–d) rotational speed, (e–h) EKE, and (i–l) radius in the Southern Ocean from 1996 to 2015. From left to right, columns represent four kinds of eddies. Black solid lines show the mean northern and southern positions of the ACC major fronts. The black dotted circle is 50° S.

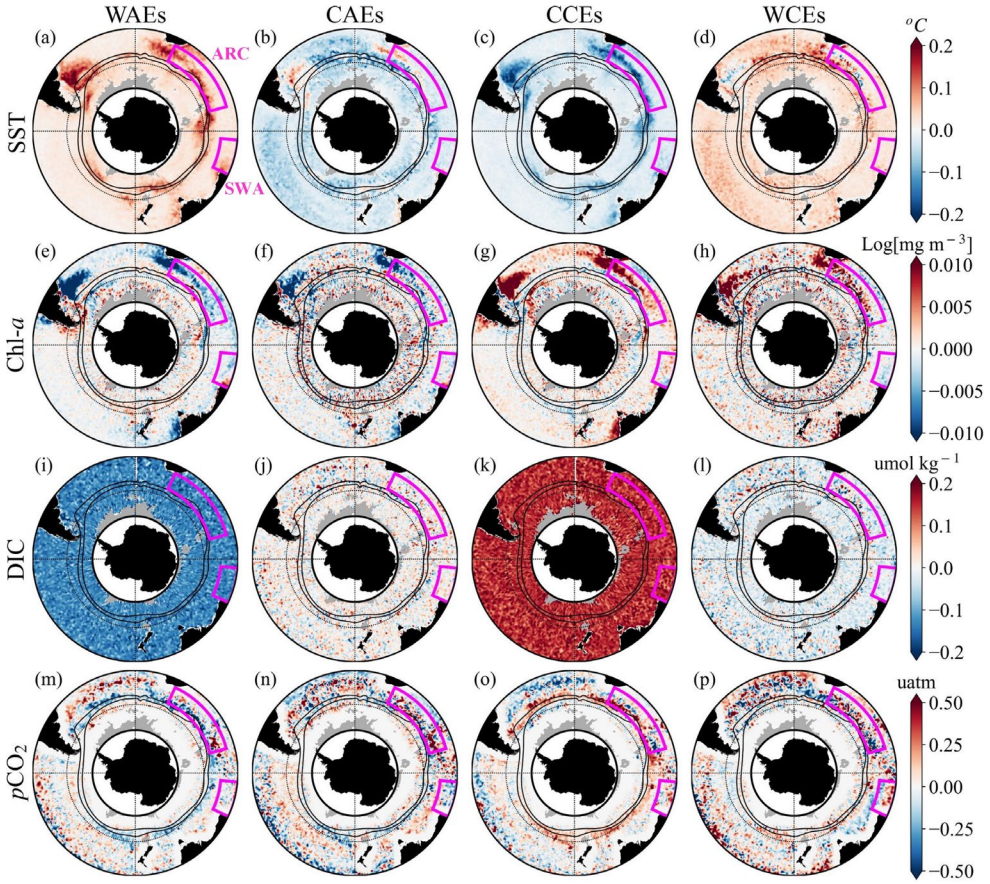
WAEs
CAEs
CCEs
WCEs
(a)
(b)
(c)
(d)
ARC
SWA
SST
°C
0.2
0.1
0.0
−0.1
−0.2
(e)
(f)
(g)
(h)
Chl-a
Log[mg m⁻³]
0.010
0.005
0.000
−0.005
−0.010
(i)
(j)
(k)
(l)
DIC
umol kg⁻¹
0.2
0.1
0.0
−0.1
−0.2
(m)
(n)
(o)
(p)
pCO2
uatm
0.50
0.25
0.00
−0.25
−0.50

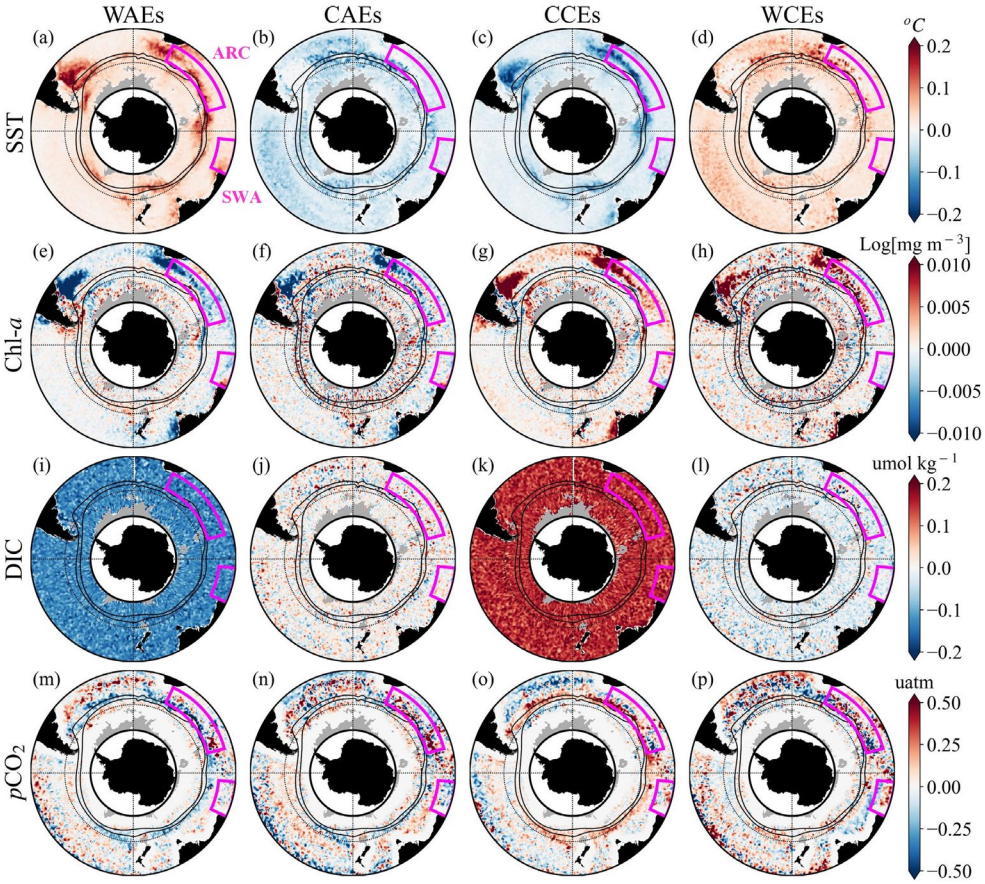

Figure 36. Spatial distribution of eddy-induced anomalies of (a–d) SST, (e–h) Chl-*a*, (i–l) DIC, and (m–p) pCO_2 in the Southern Ocean from 1996 to 2015. The anomalies within eddies are averaged in 1° × 1° longitude-latitude grid boxes. From left to right, columns represent four kinds of eddies. Black solid lines show the mean northern and southern positions of the ACC major fronts. The black dotted circle is 50° S. The magenta boxes represent ARC and SWA regions.

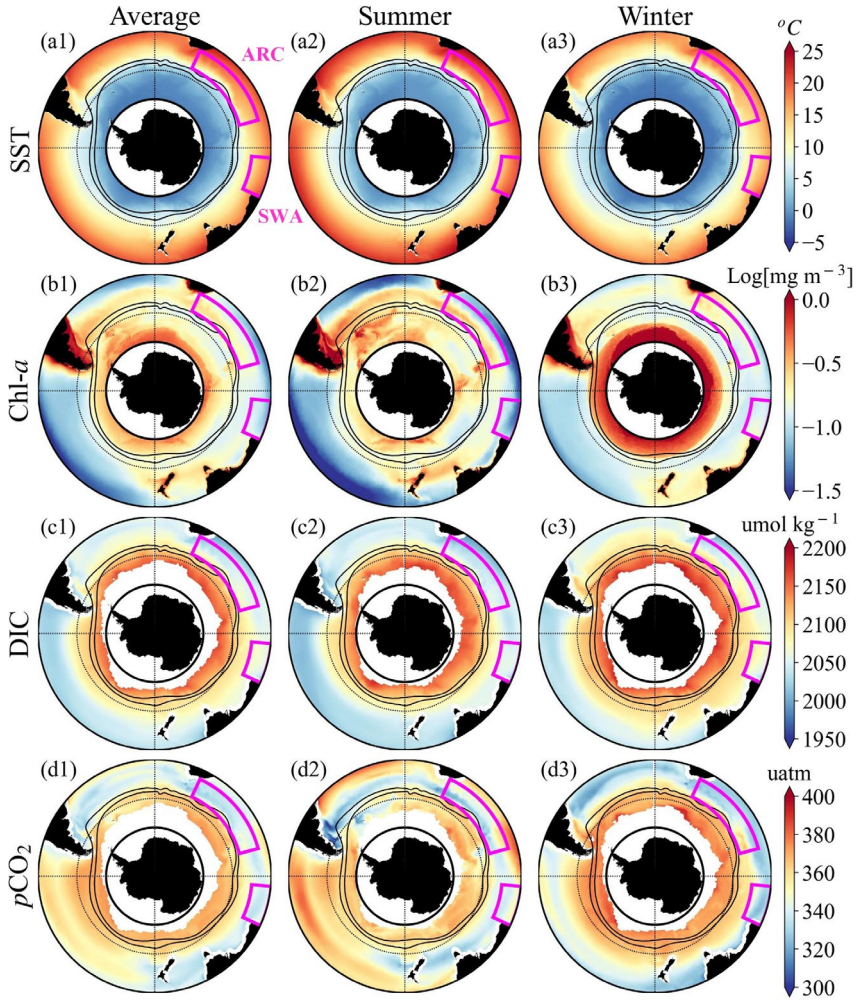
Average
Summer
Winter
(a1)
(a2)
(a3)
ARC
SWA
SST
^{o}C
25
20
15
10
5
0
−5
(b1)
(b2)
(b3)
Chl-a
Log[mg m^{-3}]
0.0
−0.5
−1.0
−1.5
(c1)
(c2)
(c3)
DIC
umol kg^{-1}
2200
2150
2100
2050
2000
1950
(d1)
(d2)
(d3)
pCO$_2$
uatm
400
380
360
340
320
300

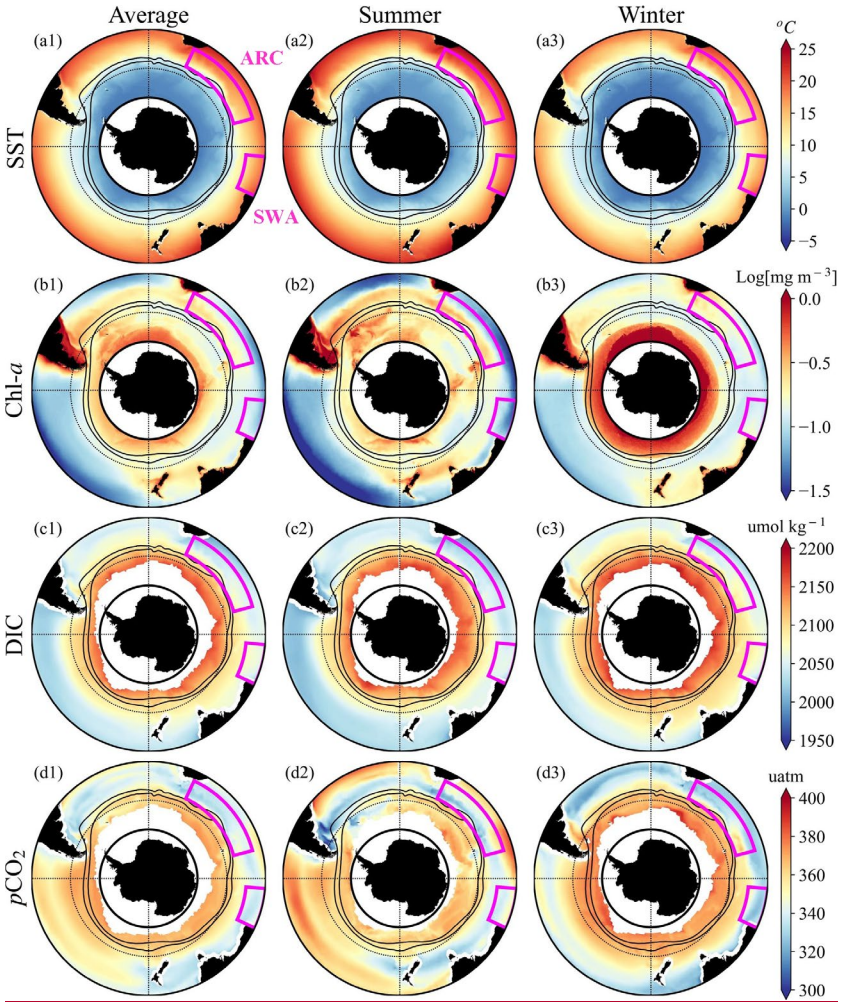

Figure 4~~7~~. The climatological~~climatology~~ and seasonal averages of (a1–a3) SST, (b1–b3) Chl-*a*, (c1–c3) DIC, and (d1–d3) pCO_2 from 1996 to 2015 in the SO. Black solid lines show the mean northern and southern positions of the ACC major fronts. The black dotted circle is 50° S. The magenta boxes represent ARC and SWA regions.

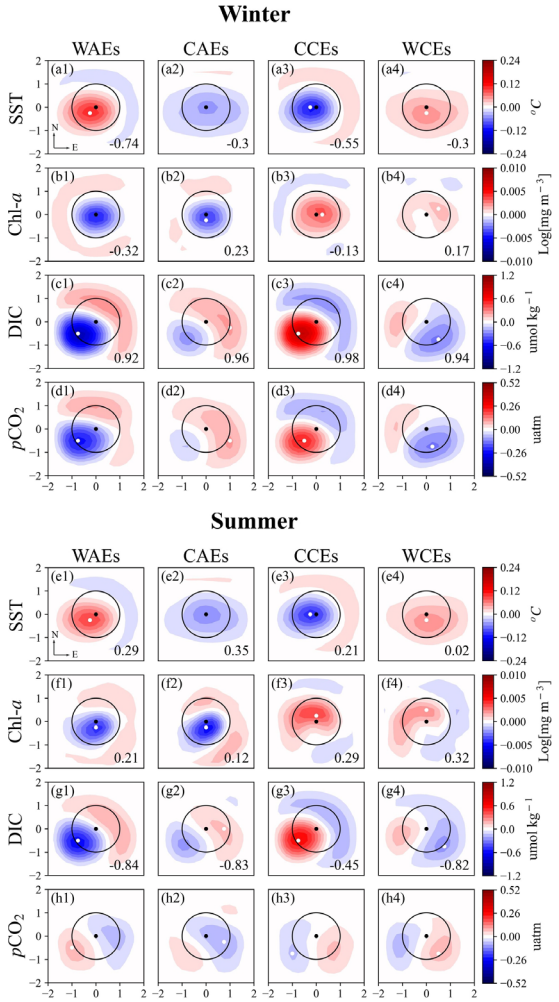
Winter
WAEs
CAEs
CCEs
WCEs
SST
Chl-a
DIC
pCO2
(a1)
(a2)
(a3)
(a4)
(b1)
(b2)
(b3)
(b4)
(c1)
(c2)
(c3)
(c4)
(d1)
(d2)
(d3)
(d4)
-0.74
-0.3
-0.55
-0.3
-0.32
0.23
-0.13
0.17
0.92
0.96
0.98
0.94
°C
Log[mg m−3]
umol kg−1
uatm
Summer
(e1)
(e2)
(e3)
(e4)
(f1)
(f2)
(f3)
(f4)
(g1)
(g2)
(g3)
(g4)
(h1)
(h2)
(h3)
(h4)
0.29
0.35
0.21
0.02
0.21
0.12
0.29
0.32
-0.84
-0.83
-0.45
-0.82
N
E

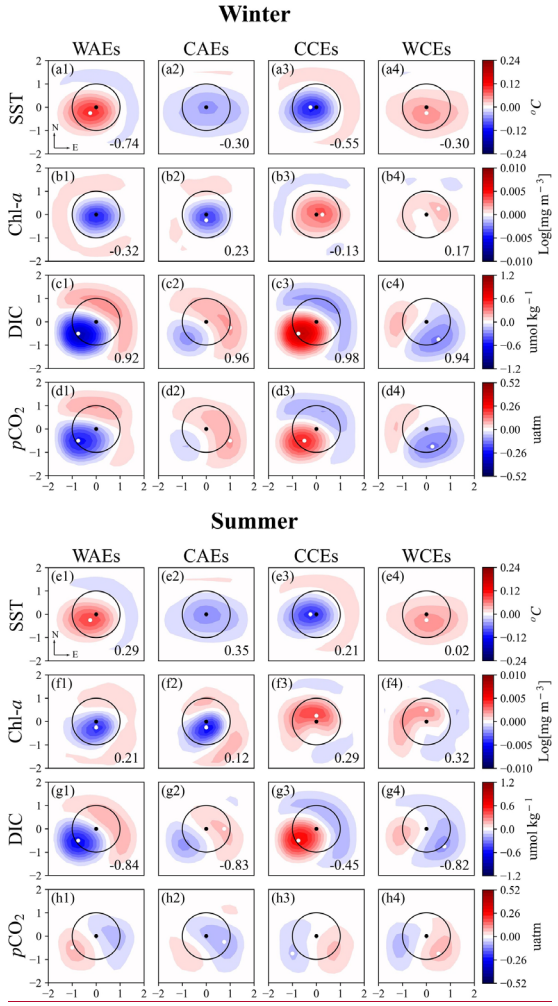

Figure 58. Eddy-centric composite averages for SST, Chl-*a*, DIC, and pCO_2 anomalies in the SO. On each map, a black dot denotes the eddy center, and a white dot denotes the center location of variables (defined by the location of the extremum value). Contour intervals are every 0.009 °C for SST, every 0.0007 Log[mg m^{-3}] for Chl-*a*, every 0.08 umol kg^{-1} for DIC, and every 0.035 uatm for pCO_2. The numbers in the lower right corner are the SSIMs.

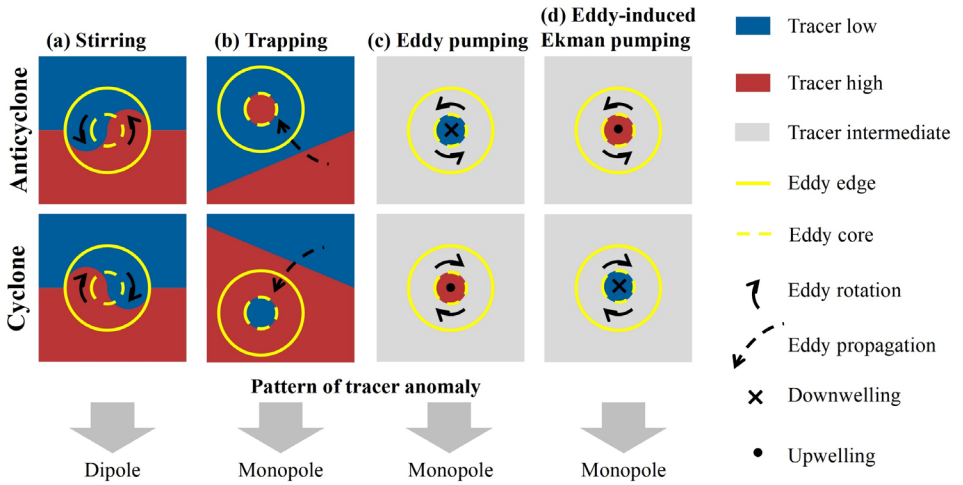

Figure 69. Schematic illustrating the mechanisms of how anticyclonic (top row) and cyclonic eddies (bottom row) affect physical and ~~biochemical~~biogeochemical parameters in the SO, including (a) eddy stirring, (b) eddy trapping, (c) eddy pumping, and (d) eddy-induced Ekman pumping. The patterns of SST anomalies induced by vertical pumping are opposite to the corresponding patterns shown in this schematic. Figure inspired by Frenger et al. (2018), Fig. 1.

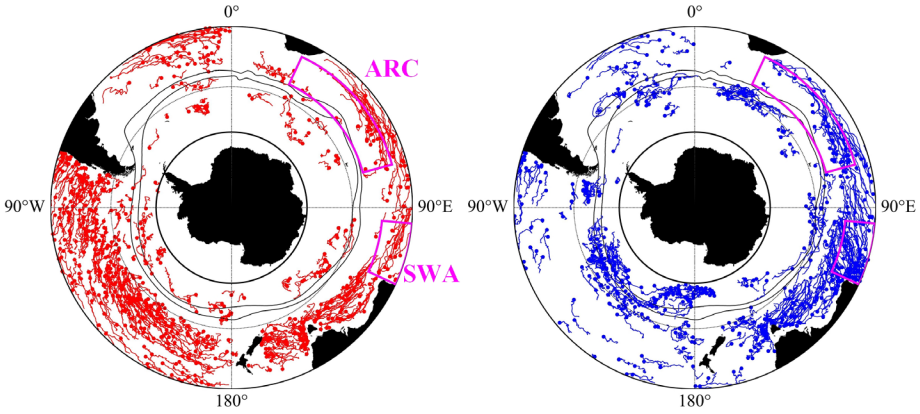

Figure 7~~10~~. Trajectories of (a) AEs and (b) CEs in the SO during 1996–2015. Red (blue) dots and lines mark the AEs (CEs) birth locations and propagation paths. Only eddies with a minimum lifetime of 1 year are considered. To show the eddies tracks more clearly, only one-third of the long-lived eddies in the south and southwest of Australia have been considered. Black solid lines show the mean northern and southern positions of the ACC major fronts. The black dotted circle is 50° S. The magenta boxes represent ARC and SWA regions.

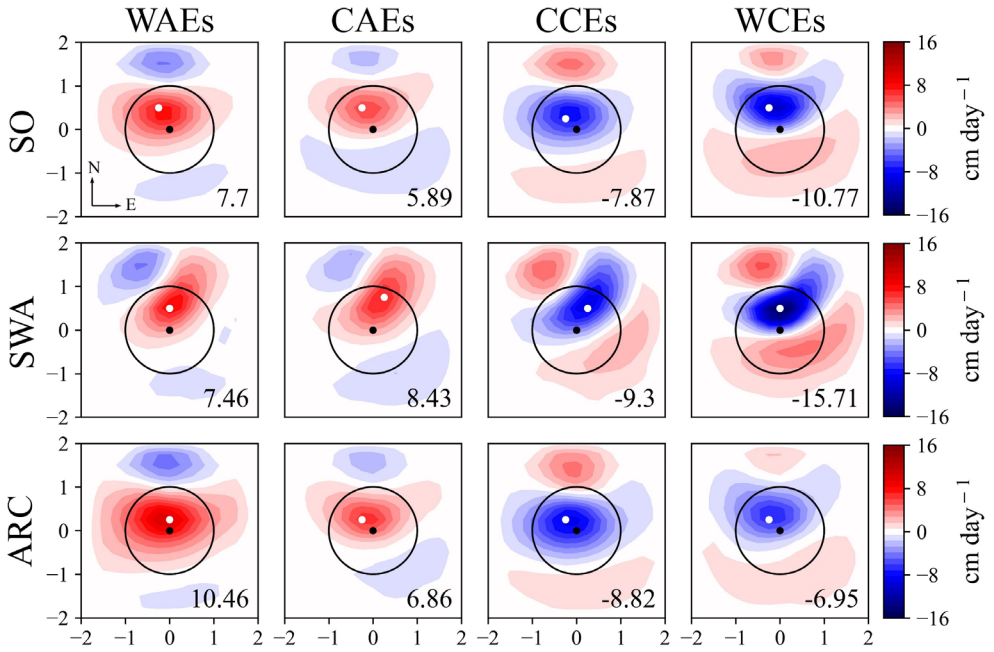
WAEs
CAEs
CCEs
WCEs
SO
SWA
ARC
N
E
7.7
5.89
-7.87
-10.77
7.46
8.43
-9.3
-15.71
10.46
6.86
-8.82
-6.95
cm day⁻¹

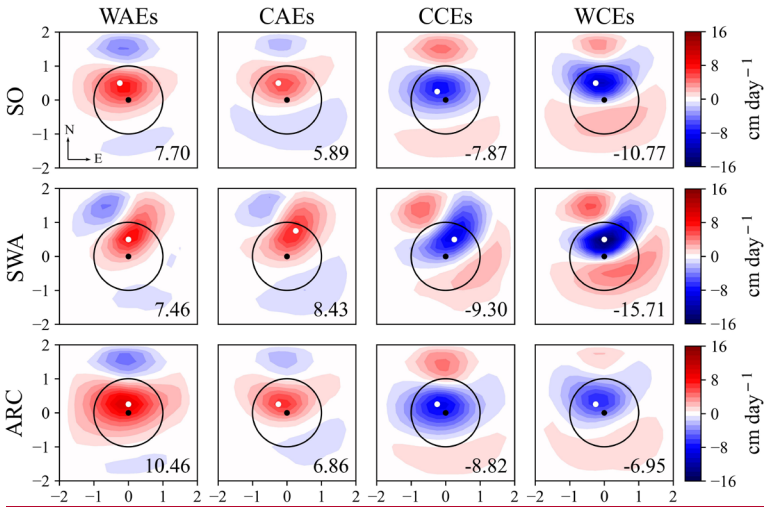

Figure 8~~11~~. Eddy-centric composite averages for eddy-induced Ekman pumping in the SO, SWA, and ARC. On each map, a black dot denotes the eddy center, and a white dot denotes the center location of variables (defined by the location of the extremum value). Contour intervals are 1.067 cm day^{-1}. The numbers in the lower right corner are the extremum value.

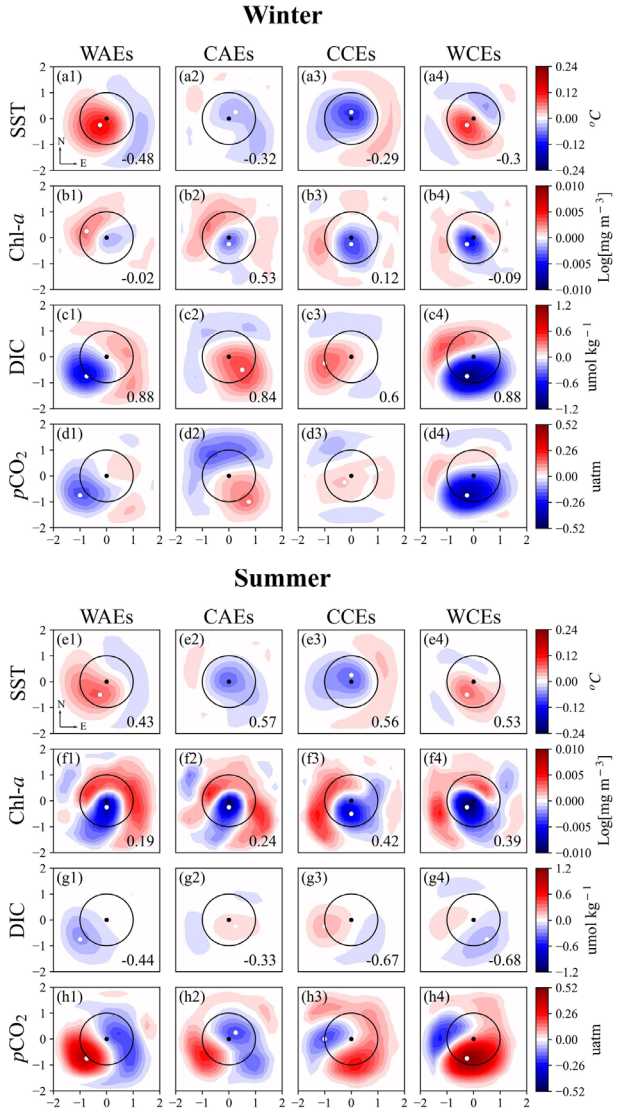
Winter
WAEs
CAEs
CCEs
WCEs
SST
Chl-a
DIC
pCO2
(a1)
(a2)
(a3)
(a4)
(b1)
(b2)
(b3)
(b4)
(c1)
(c2)
(c3)
(c4)
(d1)
(d2)
(d3)
(d4)
-0.48
-0.32
-0.29
-0.3
-0.02
0.53
0.12
-0.09
0.88
0.84
0.6
0.88
°C
Log[mg m−3]
umol kg−1
uatm
Summer
(e1)
(e2)
(e3)
(e4)
(f1)
(f2)
(f3)
(f4)
(g1)
(g2)
(g3)
(g4)
(h1)
(h2)
(h3)
(h4)
0.43
0.57
0.56
0.53
0.19
0.24
0.42
0.39
-0.44
-0.33
-0.67
-0.68
N
E

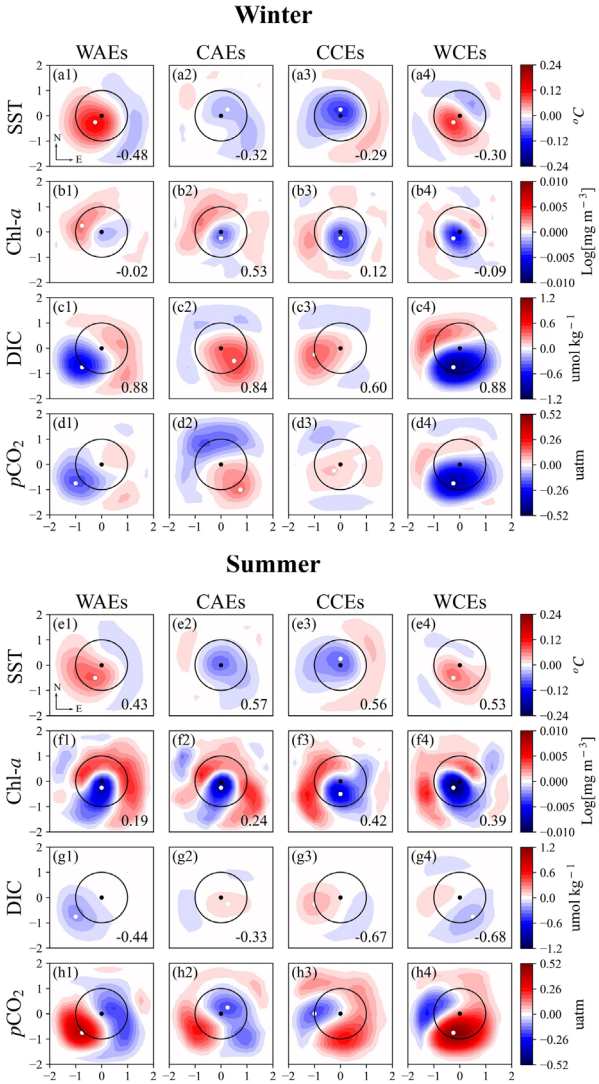

Figure 9~~12~~. Same as Fig. 5~~8~~ but for the SWA.

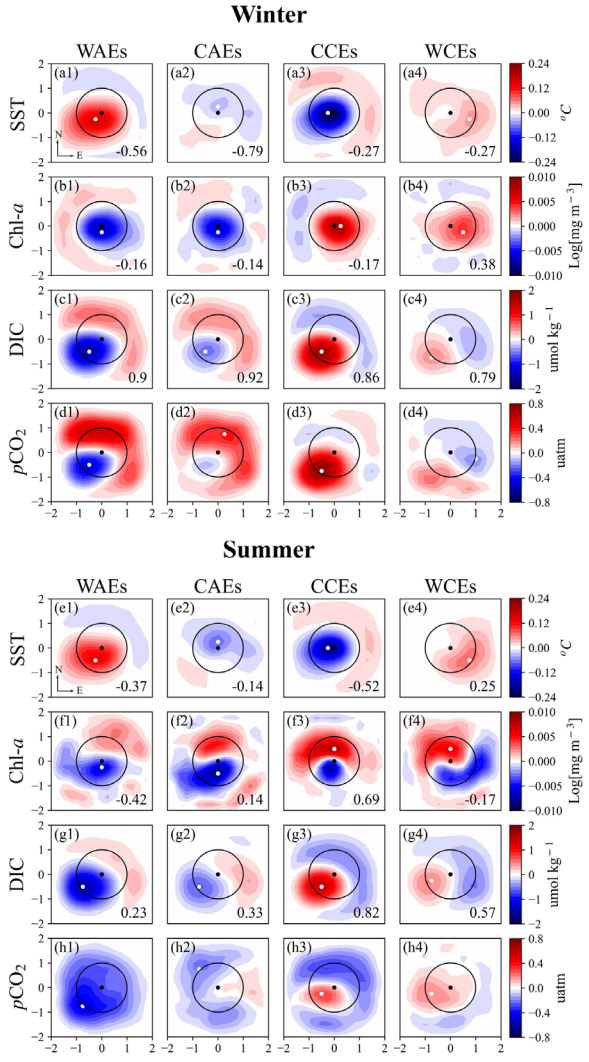
Winter
WAEs
CAEs
CCEs
WCEs
SST
Chl-a
DIC
pCO2
(a1)
(a2)
(a3)
(a4)
(b1)
(b2)
(b3)
(b4)
(c1)
(c2)
(c3)
(c4)
(d1)
(d2)
(d3)
(d4)
-0.56
-0.79
-0.27
-0.27
-0.16
-0.14
-0.17
0.38
0.9
0.92
0.86
0.79
°C
Log[mg m⁻³]
umol kg⁻¹
uatm
Summer
(e1)
(e2)
(e3)
(e4)
(f1)
(f2)
(f3)
(f4)
(g1)
(g2)
(g3)
(g4)
(h1)
(h2)
(h3)
(h4)
-0.37
-0.14
-0.52
0.25
-0.42
0.14
0.69
-0.17
0.23
0.33
0.82
0.57

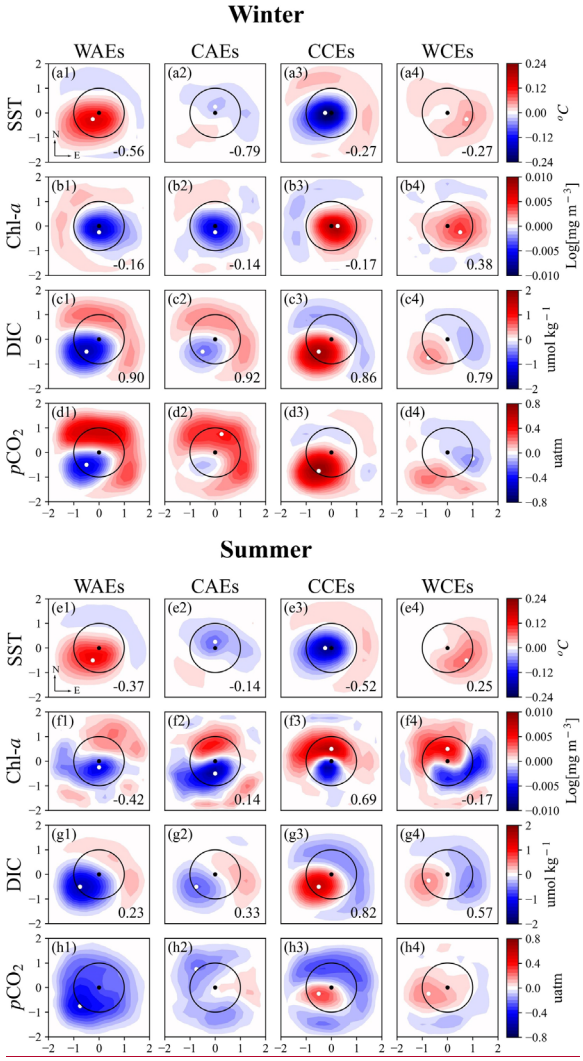

Figure 10~~3~~. Same as Fig. ~~5~~8 but for the ARC. And contour intervals are every 0.133 umol kg^{-1} for DIC and every 0.053 uatm for pCO_2.

Table 1. Significance magnitudes of effects for eddy-driven mechanisms on SST, Chl-*a*, and DIC. A indicates a dominant effect. B represents an effect that contributes to the eddy-induced anomalies but is not the dominant effect. C denotes an effect that is not significant.

	SST		Chl-*a*		DIC	
	Normal	"Abnormal"	Normal	"Abnormal"	Normal	"Abnormal"
Eddy trapping	C	C	C	C	C	C
Eddy stirring	B	C	A	A	A	A
Eddy pumping	A	B	A	A	A	B
Eddy-induced Ekman pumping	B	A	B	B	B	A

~~**Table 1.** The climatological characteristics of mesoscale eddies in the Southern Ocean from 1996 to 2015.~~

	~~WAEs/ CAEs~~	~~CCEs/WCEs~~	~~Normal /Abnormal~~	~~AEs /CEs~~
~~Number~~	~~5450860/1786338~~	~~5261780/2043428~~	~~10712640/3829766~~	~~7237198/7305208~~
~~Amplitude (cm)~~	~~6.45/6.37~~	~~6.98/6.45~~	~~6.72/6.41~~	~~6.43/6.95~~
~~Rotational speed (cm s^{-1})~~	~~15.76/15.37~~	~~16.64/16.13~~	~~16.20/15.75~~	~~15.63/16.62~~
~~EKE ($cm^2 s^{-2}$)~~	~~83.78/85.90~~	~~105.88/102.86~~	~~94.83/94.38~~	~~83.95/106.29~~
~~Radius (km)~~	~~88.62/87.24~~	~~87.54/82.96~~	~~88.08/85.10~~	~~88.82/87.21~~

Table 2. Contributions of eddies to pCO_2 in different regions and seasons from 1996 to 2015. The contributions are the percentages of the eddy-induced pCO_2 anomalies maximum to the intra-annual variation of the corresponding variables.

Region	Eddy Type	Annual (%)	Winter (%)	Summer (%)
SO	WAEs	−0.87	−2.64	0.75
	CAEs	−0.27	1.04	−0.97
	CCEs	0.91	2.5	−0.67
	WCEs	−0.39	−1.4	0.8
SWA	WAEs	1.4	−1.76	4.12
	CAEs	−1.55	1.53	−2.06
	CCEs	−0.88	0.61	−1.91
	WCEs	1.49	−3.99	5.15
ARC	WAEs	−2.49	−3.15	−3.12
	CAEs	1.03	2.52	−1.4
	CCEs	2.53	5.03	2.06
	WCEs	−0.89	−1.19	1.26